Check for updates

System Identification for Small Flying-Wing Unmanned Aircraft Using Open-Loop and Closed-Loop Flight Data

Justin J. Matt,* Haiyang Chao,† Mosarruf H. Shawon,‡ and Benjamin C. Svoboda§
University of Kansas, Lawrence, Kansas 66045
and
Steven G. Hagerott¶
Textron eAviation, Wichita, Kansas 67218

https://doi.org/10.2514/1.C038147

Small unmanned aircraft systems (sUAS) face unique challenges in system identification due to their lightweight, small size, and increased sensitivity to wind and gusts. To address these challenges, flight test procedures for sUAS system identification using open-loop and closed-loop flight data are presented. The approaches are demonstrated through system identification of a small flying-wing UAS equipped with a low-cost Pixhawk autopilot. The open-loop method is demonstrated through identification of the longitudinal bare-airframe aircraft dynamics. Longitudinal frequency responses were estimated from the open-loop flight data, and a linear state space model was identified from the estimated frequency responses and supplemental trim data, which was used to better identify parameters related to the low-frequency phugoid mode. The identified phugoid mode matches well with low-frequency oscillations measured from flight data in the time domain. The closed-loop method is demonstrated through identification of the lateral-directional dynamics. This approach is shown to improve the signal-to-noise ratio and reduce deviation from the reference flight condition, which improves modeling results, and it can be used to simultaneously identify the bare-airframe, closed-loop, and broken-loop UAS dynamics from the same set of closed-loop flight data, reducing time and efforts spent flight testing. The identified lateral-directional model is compared with closed- and broken-loop frequency responses estimated from flight data. The results show excellent agreement, with all computed metrics, such as stability margins, matching within 10%, demonstrating the effectiveness of this method.

Downloaded by NASA LANGLEY RESEARCH CENTER on March 17, 2025 | http://arc.aiaa.org | DOI: 10.2514/1.C038147

Nomenclature

a_x, a_y, a_z	=	body x-, y-, and z-axis accelerometer measurements, m/s^2
g	=	gravitational acceleration, m/s^2
G	=	single-input, single-output dynamic model
J	=	cost function value
$L_{[\cdot]}, M_{[\cdot]}, N_{[\cdot]}$	=	dimensional roll, pitch, and yaw moment stability and control derivatives
n	=	motor rotational speed, rev/s
p, q, r	=	roll, pitch, and yaw rates, rad/s or deg /s
r_c	=	reference command signal
S_{uu}, S_{yy}, S_{uy}	=	input autospectra, output autospectra, and input–output cross spectra
u, v, w	=	perturbation x-, y-, and z-body axis velocities, m/s
U_0, W_0, Θ_0	=	trim x-body velocity, z-body velocity, and pitch angle
$X_{[\cdot]}, Y_{[\cdot]}, Z_{[\cdot]}$	=	dimensional body-axis force stability and control derivatives
γ^2_{uy}	=	coherence function
δ_a, δ_e	=	aileron and elevator deflections, rad or deg
$\delta_{a_c}, \delta_{e_c}$	=	aileron and elevator commands
$\zeta, \omega_d, \omega_n$	=	damping coefficient, damped natural frequency (rad/s), and undamped natural frequency, rad/s
$\tau_{\delta_e}, \tau_{\delta_a}, \tau_n$	=	time delay of elevator, aileron, and motor speed inputs, s
ϕ, θ	=	perturbation roll and pitch attitudes, rad or deg
ϕ_c	=	roll angle command, rad or deg

Received 18 July 2024; accepted for publication 31 December 2024; published online 7 March 2025. Copyright © 2025 by Justin J. Matt, Haiyang Chao, Mosarruf H. Shawon, Benjamin C. Svoboda, and Steven G. Hagerott. Published by the American Institute of Aeronautics and Astronautics, Inc., with permission. All requests for copying and permission to reprint should be submitted to CCC at www.copyright.com; employ the eISSN 1533-3868 to initiate your request. See also AIAA Rights and Permissions www.aiaa.org/randp.

*M.S. Student, Department of Aerospace Engineering; justinjmatt@gmail.com.
†Associate Professor, Department of Aerospace Engineering; chaohaiyang@ku.edu.
‡Ph.D. Student, Department of Aerospace Engineering.
§Undergraduate Student, Department of Aerospace Engineering.
¶Flight Controls and Aeromechanics Principal Engineer.

I. Introduction

UNMANNED aircraft systems (UAS) have become increasingly important platforms for the research and development of next-generation autonomous aircraft, such as urban air mobility and autonomous cargo delivery vehicles. A significant step in the development of UAS is the identification of dynamic models from flight data using system identification techniques. These models are critical to many applications, such as controller design or flight simulation. System identification techniques have been extensively developed for and applied to manned aircraft problems [1–3]. Compared with larger aircraft, however, it is often difficult to perform high-accuracy system identification for small UAS (sUAS), partially due to their low speeds and lightweight. Small UAS are more sensitive to atmospheric disturbances than larger aircraft, which may result in noisy measurement data and necessitate larger, less stable flight maneuvers to achieve high signal-to-noise ratios (SNRs) needed for accurate identification [4,5]. Atmospheric disturbances also create difficulties with data collection from repeated maneuvers at the same flight condition or from long-duration maneuvers, which are also important for accurate model identification results. These challenges point to a need for an easily repeatable system identification procedure tailored specifically to sUAS.

In recent years, several works have successfully applied system identification approaches to sUAS, including time- and frequency-domain methods [4–13]. A few of these works developed new procedures to address some of the sUAS-specific challenges mentioned previously. For example, wind tunnel test data [8] and vortex lattice method analysis [7] have been used to supplement flight-test-based system identification results to better identify the low-frequency phugoid dynamics, which are challenging to identify

Downloaded by NASA LANGLEY RESEARCH CENTER on March 17, 2025 | http://arc.aiaa.org | DOI: 10.2514/1.C038147

from flight maneuver data. In [7], brief multistep maneuvers were flown to address the difficulty of having a ground-based pilot fly long maneuvers at a desired flight condition. In prior work [4,6], recommendations were made for flight testing techniques to address these challenges and ensure the collection of high-quality system identification data. The methods proposed in this paper are a summary and an extension of this work.

Another potential approach to address constraints encountered during sUAS system identification flight tests is through closed-loop flight testing. Historically, open-loop flight testing has been preferred because, for larger, manned aircraft, the disadvantages of closed-loop testing outweighed the benefits. Namely, automatic flight control systems may suppress excitation, especially if there is integral action, or create undesirable correlation between multiple inputs or between inputs and noise and disturbances, which can degrade model identification results. Despite these drawbacks, however, there are numerous benefits to studying closed-loop system identification. For example, closed-loop testing may be required for safety reasons or for unstable aircraft such as multirotor or electric vertical takeoff and landing (eVTOL) sUAS. Additionally, the unique challenges of sUAS system identification can be well-addressed through closed-loop testing. Closed-loop testing increases stability during system identification flight maneuvers, which allows for larger maneuvers and thus larger SNRs needed for accurate results. Closed-loop testing also greatly improves the ability to achieve and maintain a desired flight condition during maneuvers, which is needed to collect repeated data sets for modeling or separate data sets for model validation tests. Moreover, closed-loop operation can reduce the total flight test time, as bare-airframe, closed-loop, and broken-loop system dynamics can all be identified from the same set of flight data [14,15], rather than from separate open- and closed-loop data sets. This is particularly useful as many sUAS are equipped with capable flight control systems that can be easily tuned during initial flight tests [16], making it feasible to perform system identification during one of the first flights of a new vehicle. In summary, closed-loop flight testing can improve the stability, repeatability, and efficiency of flight tests for sUAS system identification, making it an attractive option for flight test design.

System identification from closed-loop flight data has been investigated less than with open-loop data, due to the aforementioned disadvantages caused by control systems. Several authors have used parametric modeling techniques to identify bare-airframe models for multirotor sUAS from closed-loop data [17–19]. Others have applied conventional spectral methods to estimate nonparametric bare-airframe frequency response models from closed-loop data for both multirotor [20–22] and fixed-wing sUAS [10]. This approach of directly estimating frequency responses is biased, although good results can still be obtained if the bias is small, which is achieved through high SNRs [1]. This bias can be resolved by estimating frequency responses indirectly using a joint input–output (JIO) method [23–25]. In a prequel to this work [14], the JIO approach for estimating frequency responses from closed-loop sUAS flight data was demonstrated through simulation. The JIO method has also been applied to system identification problems for small multirotor aircraft and manned aircraft with multiple inputs that are highly correlated due to feedback or mixing [24,26–29]. Similarly, in [30], the input correlation problem was addressed for orthogonal multisine inputs using an interpolation technique.

Other works have focused on using closed-loop flight data to identify models of the closed-loop system. In [15], a technique was demonstrated using simulation data to identify bare-airframe, closed-loop, and broken-loop frequency responses simultaneously by injecting multiple signals with different, discrete harmonics at various points in the flight control system of a full-scale aircraft. Similarly, in a prequel to this work [14], a method to simultaneously identify these frequency responses from a single excitation signal was demonstrated through simulation, and the specific advantages of this method for fixed-wing sUAS were discussed. In [12], closed-loop flight testing was conducted to estimate closed-loop and broken-loop frequency responses for an sUAS. The estimated frequency responses were compared with a bare-airframe model obtained from separate open-loop flight test data, which is a common practice for control system design [31]. Generally, however, system identification from closed-loop flight data for small fixed-wing UAS has seldom been studied, and the explicit benefits to modeling and flight test efficiency have not been explored.

In this paper, a comprehensive procedure is developed to address the unique challenges of sUAS bare-airframe system identification using frequency response-based methods. The procedure is an extension of the work in [4,6,14] and includes methods for performing system identification through open-loop and closed-loop flight testing, and the advantages and disadvantages of each method are discussed. The proposed methods are demonstrated using a small flying-wing UAS, which faces complications during system identification flight testing due to its lightweight, low stability, and lack of yaw control. We first present practical approaches for sUAS experiment design to efficiently collect data for system identification, including flight data from frequency sweep maneuvers, multistep maneuvers, and trimmed steady-state flight and bench test data to identify actuator dynamics. Decoupled linear longitudinal and lateral-directional dynamic models were identified from these data sets. Longitudinal modeling results were obtained using the developed open-loop method, which utilizes trim data and frequency responses identified from open-loop flight data to identify a model characterizing both the short-period and phugoid modes. This method also includes a second approach for identifying the phugoid mode dynamics from oscillations measured in the time domain, which is a novel result in the sUAS literature. Lateral-directional modeling results were obtained using the developed closed-loop method. The JIO method was used to estimate bare-airframe frequency responses from closed-loop data. The closed-loop method is particularly useful for sUAS that face challenges repeating system identification maneuvers at the same flight condition. This approach is also highly efficient, as the sUAS bare-airframe, closed-loop, and broken-loop system dynamics are identified from the same set of flight data through simple attitude command maneuvers, potentially further reducing flight test time. The closed-loop maneuvers can be performed by a human pilot or autopilot with a single excitation signal. Because of these benefits, the developed closed-loop method can reduce the time, effort, and cost of sUAS system identification flight testing.

This paper is organized as follows: Section II describes the sUAS system identification problem and overall procedure. Section III outlines the sUAS flight test platform and mathematical structures used for modeling. Flight test design and model identification approaches are described in Secs. IV and V. Section VI presents system identification results and a discussion on the tradeoffs between the open-loop and closed-loop approaches. Finally, Sec. VII provides concluding remarks and future directions.

II. Problem Description

This paper focuses on the identification of bare-airframe and closed-loop system dynamics for a small flying-wing UAS using frequency-response-based approaches. The proposed system identification procedure is summarized in Fig. 1, which includes methods for using open-loop or closed-loop flight maneuver data. Both methods are demonstrated, and the advantages and disadvantages of each are discussed.

The open-loop method, shown on the left-hand side of Fig. 1, begins with the collection of system identification data from open-loop flight test maneuvers such as frequency sweeps. This data can be used to estimate bare-airframe frequency responses and identify a parametric model from open-loop maneuver data alone or in combination with supplemental data, such as trim data used to improve phugoid modeling results. As a demonstration, this paper uses this method to identify a parametric longitudinal dynamic model that accurately characterizes both the short-period and phugoid modes. The identified model can then be compared against supplemental data that was not used in system identification for validation, such as doublet data and phugoid oscillation data. It is worth noting that, although supplemental data may be collected open- or closed-loop

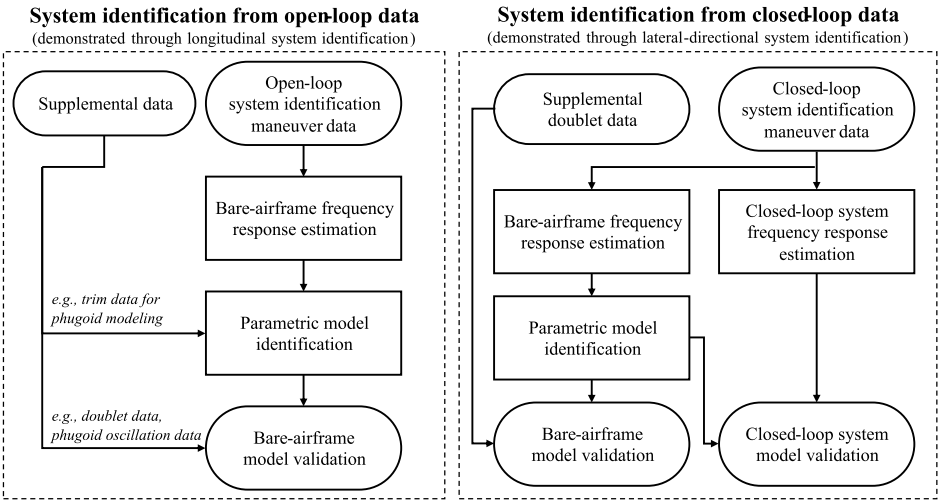

Fig. 1 Procedures for frequency-response-based UAS system identification.

depending on the application, the method is referred to as the "open-loop method" because the primary data used for modeling is collected open-loop.

Often following identification of a bare-airframe model, flight control systems are designed, and closed-loop system identification flight testing is conducted to validate the implementation of the digital control system [1,12,31]. This can be achieved by comparing the modeled closed-loop and broken-loop transfer functions (and important metrics derived from them, such as stability margins) with the equivalent frequency responses measured from flight data. This process aligns with typical design cycles for large aircraft, as control systems are often designed using models identified from open-loop system identification flight testing. However, many small UAS are equipped with flight control systems that can be tuned in flight without a model. In this paper, the closed-loop approach, shown on the right-hand side of Fig. 1, was developed to demonstrate the benefit of conducting closed-loop flight testing for data collection for both bare-airframe and closed-loop system identification. This can reduce flight testing from a two-step process, where both open- and closed-loop system identification maneuver data is collected, to a single campaign where closed-loop system identification maneuver data is used to estimate frequency responses of both the bare-airframe and the closed-loop system dynamics. The bare-airframe frequency responses can be used to identify a parametric model, and the closed-loop system frequency responses can be compared against a closed-loop model that is developed from the identified bare-airframe model and knowledge of the control system.

One advantage of the closed-loop method is reduced time and efforts spent collecting flight data, as open-loop frequency sweep data does not need to be collected. Furthermore, for sUAS that are sensitive to atmospheric disturbances, closed-loop testing can improve repeatability and data quality for system identification. This approach is also suitable for unstable aircraft that require an active flight control system at all times, such as multirotor sUAS. In this work, both the open-loop and closed-loop methods are demonstrated using a small flying-wing UAS. The open-loop method was used for longitudinal bare-airframe system identification, as maneuvers around this axis are more stable, whereas the closed-loop method was used for lateral-directional bare-airframe and closed-loop system identification.

III. UAS Platform and Model Structures

A. UAS Platform

The system identification procedure was performed using the KHawk Zephyr3-R UAS, which was developed at the Cooperative Unmanned Systems Laboratory (CUSL) at the University of Kansas. The Zephyr3-R, shown in Fig. 2, is a flying-wing UAS constructed from a commercial-off-the-shelf RiteWing Zephyr III Wing airframe. The vehicle has two elevons and a brushless electric motor

Fig. 2 KHawk Zephyr3-R UAS.

as control inputs. The elevons are controlled by mixing the aileron, δ_a, and elevator, δ_e, commands generated by a human pilot or autopilot via Eqs. (1) and (2), where a positive value indicates deflection of the elevon trailing edge downward. Two Spektrum A5040 mini digital servos are used for the control of elevons.

$$\delta_{\text{elevon}_{\text{left}}} = 0.5(\delta_e + \delta_a) \tag{1}$$

$$\delta_{\text{elevon}_{\text{right}}} = 0.5(\delta_e - \delta_a) \tag{2}$$

The UAS is controlled by a Cube Black Pixhawk autopilot running customized ArduPlane** open-source firmware. The Cube contains three redundant, internal inertial measurement units (IMUs) and interfaces with peripheral devices for sensing, command generation, telemetry, and data logging. A GPS receiver and an airspeed sensor provide position, inertial velocity, and airspeed measurement. IMU and command signal data was used for system identification and recorded at 100 Hz. The electric motor speed is measured by a Castle Creations Electronic Speed Controller (ESC) at 10 Hz and interpolated to 100 Hz for data processing. Specifications of the KHawk Zephyr3-R are shown in Table 1.

B. Bare-Airframe UAS Dynamic Model Structures

Aircraft dynamics can be represented using nonparametric or parametric models for different applications. Nonparametric models include frequency response or other data-based representations. Different parametric model structures can be used for sUAS dynamic modeling, including linear single/multi-input, single/multi-output (SISO/SIMO/MISO/MIMO) models, or nonlinear models. Linearized

**See more at https://ardupilot.org/ [retrieved 18 April 2024].

Downloaded by NASA LANGLEY RESEARCH CENTER on March 17, 2025 | http://arc.aiaa.org | DOI: 10.2514/1.C038147

Downloaded by NASA LANGLEY RESEARCH CENTER on March 17, 2025 | http://arc.aiaa.org | DOI: 10.2514/1.C038147

Table 1 KHawk Zephyr3-R UAS specifications

Parameter	Value
Mass, kg	2.18
Wingspan, cm	122
Cruise speed, m/s	15–25
Mean aerodynamic chord, cm	31
Wing area, m^2	0.413

models are the primary focus of this paper as they provide an accurate representation of sUAS dynamics around a trim condition and allow for frequency response-based analysis, which is often beneficial for control system design and for gaining physical understanding of the system. Longitudinal and lateral-directional dynamics are assumed to be decoupled, as is common with fixed-wing aircraft, and identified separately. This subsection outlines the bare-airframe dynamic model structures used for system identification.

1. Longitudinal Bare-Airframe Dynamics

The longitudinal bare-airframe dynamics can be represented using nonparametric frequency responses between the longitudinal inputs and outputs. They can also be modeled parametrically using a linear state space model, representing the longitudinal dynamics around a trimmed reference flight condition [1]:

$$\begin{bmatrix} \dot{u} \\ \dot{w} \\ \dot{q} \\ \dot{\theta} \end{bmatrix} = \begin{bmatrix} X_u & X_w & X_q - W_0 & -g\cos\Theta_0 \\ Z_u & Z_w & Z_q + U_0 & -g\sin\Theta_0 \\ M_u & M_w & M_q & 0 \\ 0 & 0 & 1 & 0 \end{bmatrix} \begin{bmatrix} u \\ w \\ q \\ \theta \end{bmatrix} + \begin{bmatrix} X_{\delta_e} & X_n \\ Z_{\delta_e} & Z_n \\ M_{\delta_e} & M_n \\ 0 & 0 \end{bmatrix} \begin{bmatrix} \delta_e(t-\tau_{\delta_e}) \\ n(t-\tau_n) \end{bmatrix} \tag{3}$$

where u is the x-axis body velocity, w is the z-axis body velocity, θ is the pitch angle, δ_e is the elevator deflection, and n is the motor rotational speed. U_0, W_0, and Θ_0 are the trim x- and z-axis body velocities and trim pitch angle, g is gravitational acceleration, and τ_{δ_e} and τ_n are system time delays for elevator and motor speed inputs. All states and controls are perturbation values. The $X_{[\cdot]}$, $Z_{[\cdot]}$, and $M_{[\cdot]}$ terms are the longitudinal dimensional stability and control derivatives to be identified.

2. Lateral-Directional Bare-Airframe Dynamics

Similarly, the lateral-directional UAS dynamics can be represented as nonparametric frequency responses for each input–output pair and as a linear state space model at a prescribed flight condition [1]:

$$\begin{bmatrix} \dot{v} \\ \dot{p} \\ \dot{r} \\ \dot{\phi} \end{bmatrix} = \begin{bmatrix} Y_v & Y_p + W_0 & Y_r - U_0 & g\cos\Theta_0 \\ L_v & L_p & L_r & 0 \\ N_v & N_p & N_r & 0 \\ 0 & 1 & \tan(\Theta_0) & 0 \end{bmatrix} \begin{bmatrix} v \\ p \\ r \\ \phi \end{bmatrix} + \begin{bmatrix} Y_{\delta_a} \\ L_{\delta_a} \\ N_{\delta_a} \\ 0 \end{bmatrix} \delta_a(t-\tau_{\delta_a}) \tag{4}$$

where v is the y-axis body velocity, p and r are the roll and yaw rates, ϕ is the roll angle, δ_a is the aileron deflection, and τ_{δ_a} is the system time delay for aileron inputs. All states and controls are perturbation values. The $Y_{[\cdot]}$, $L_{[\cdot]}$, and $N_{[\cdot]}$ terms are the lateral-directional dimensional stability and control derivatives to be identified. Note that the $L_{[\cdot]}$ and $N_{[\cdot]}$ terms are lumped derivatives, which include cross-coupling between roll and yaw due to the vehicle product of inertia [1,32].

Given knowledge of the sUAS mass and inertia properties, the state space models in Eqs. (3) and (4) can also be expressed using nondimensional stability and control derivatives. These nondimensional parameters can be derived from standard equations [4,32,33] and can be useful for comparisons with computational or wind tunnel-based estimates [34].

3. Model Outputs

The primary outputs used for modeling are the body x-, y-, and z-axis accelerations (a_x, a_y, a_z) and the roll, pitch, and yaw rates (p, q, r) measured by the IMU. In this work, airflow angle measurements were not considered, as is common for sUAS due to weight and cost constraints. The body velocity derivatives were also used for modeling and were reconstructed from IMU measurements using linearized equations for small perturbations around a trim condition [1]:

$$\dot{u} = a_x - W_0 q - (g\cos\Theta_0)\theta \tag{5}$$

$$\dot{v} = a_y - U_0 r + W_0 p + (g\cos\Theta_0)\phi \tag{6}$$

$$\dot{w} = a_z + U_0 q - (g\sin\Theta_0)\theta \tag{7}$$

Note that it is necessary to check the kinematic consistency of these measurements before data analysis and system identification [1,2]. The body velocities can be reconstructed from their derivatives in the frequency domain by multiplying by a factor of $1/s$. When fitting a model to frequency responses, results are equivalent when fitting to the velocity derivative or reconstructed velocity responses [1]. In addition to these measurements, airspeed sensor data was used to estimate the trim airspeed but was not used directly for model identification due to the high noise level and slow-changing dynamics.

C. Closed-Loop System Model Structures

System identification can also be conducted to model the closed-loop system dynamics and quantify control system performance. Transfer functions can be used to model the SISO relationships of the closed-loop system, which describe the response of the UAS to reference commands, such as roll or pitch angle commands. Consider Fig. 3, which shows a generic closed-loop system that consists of the plant G and controller K. The control system drives the output y to track the reference command r_c. The inputs and outputs of relevant broken loops, obtained by opening a SISO loop at a particular point, are also labeled. These loops are of interest to flight control engineers as they can be used to analyze stability margins and the sensitivity of the aircraft to noise and disturbances [1,35,36].

Three loops of particular interest can be derived from the diagram shown in Fig. 3. First, the closed-loop transfer function from reference command to output is given by

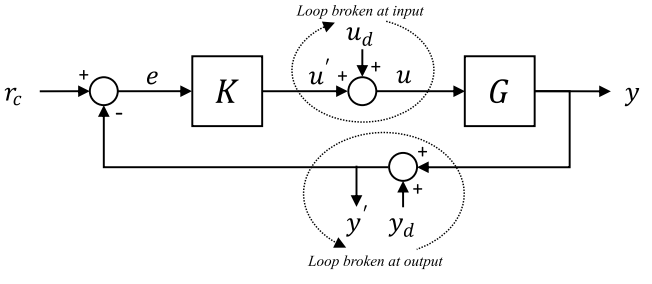

Fig. 3 Generic closed-loop system with broken loops labeled.

$$\frac{y}{r_c}(s) = \frac{G(s)K(s)}{1 + G(s)K(s)} \tag{8}$$

This loop describes the UAS response to reference commands and characterizes the closed-loop tracking ability of the vehicle.

The loop response broken at the input is also important, as the control system stability margins are measured from this response. The transfer function for this loop is given by

$$\frac{u'}{u}(s) = -K(s)G(s) \tag{9}$$

Broken loops can also be used to estimate sensitivity functions, which are often used to characterize the aircraft's ability to attenuate disturbances [36,37]. The output sensitivity function for the system in Fig. 3 is

$$\frac{y'}{y_d}(s) = [1 + G(s)K(s)]^{-1} = 1 - \frac{G(s)K(s)}{1 + G(s)K(s)} = 1 - \frac{y}{r_c}(s) \tag{10}$$

This transfer function is equal to the error response to the reference command, $e/r_c(s)$. Additionally, the second term on the right-hand side of Eq. (10) is equal to the closed-loop transfer function in Eq. (8). Two metrics, the disturbance rejection bandwidth (DRB) and disturbance rejection peak (DRP), can be computed from the output sensitivity function [31,36,37]. These metrics are often used to characterize the aircraft's response to disturbances.

Frequency responses of the closed-loop and broken-loop dynamics can be estimated from measurement data and compared with the above theoretical transfer functions derived from a closed-loop model composed of the bare-airframe dynamics and control system. This process provides a nonparametric method to verify that the closed-loop system is behaving as designed. Typical flight test measurement procedures involve injecting signals individually at each of the three labeled inputs in Fig. 3, r_c, u_d, and y_d, and then estimating the frequency response from the relevant input–output data using either direct or indirect methods [1]. In this paper, it is shown that these frequency responses can all be accurately estimated from a single sUAS flight data set acquired through reference command excitations (r_c in Fig. 3, such as roll angle commands), rather than collecting different data sets for individual signals injected at the reference command, input, and feedback path.

IV. UAS Flight Test Design and Data Collection

A critical step for UAS system identification is to collect high-quality system identification flight data, as the data quality will generally determine the accuracy of the identified models. Small flying-wing UAS pose unique challenges when designing flight test procedures for system identification data collection, and many of these challenges may not need to be considered for large UAS or manned aircraft. Challenges experienced during system identification flight testing of the Zephyr3-R include the following:

1) The small, tailless flying-wing configuration results in low stability of the open-loop dynamics.

2) Wind and atmospheric turbulence can significantly affect system identification flight testing, which causes disturbances to the aircraft response, increases the noise level, and makes it difficult to fly at consistent trim conditions.

3) Elevon control surfaces lead to increased coupling between the roll and pitch responses.

4) No direct yaw control is available through elevons.

5) Visual line-of-sight (VLOS) safety requirements limit the maximum length of system identification maneuvers. This makes it difficult to accurately identify low-frequency dynamics such as the phugoid mode dynamics.

This section describes the open- and closed-loop flight test procedures designed to address these challenges. The following flight data sets were collected to demonstrate the two proposed methods:

1) Open-loop elevator and throttle frequency sweep data was collected to estimate longitudinal bare-airframe frequency responses.

2) Closed-loop roll command frequency sweep data was collected to estimate lateral-directional bare-airframe, closed-loop, and broken-loop frequency responses.

3) Closed-loop trim data was collected to estimate the change in UAS states and controls as a function of airspeed and to identify longitudinal speed stability derivatives from this relationship, improving the accuracy of the identified phugoid mode.

4) Open-loop trim data was collected to measure the phugoid mode dynamics directly from oscillations in the UAS velocity and pitch angle.

5) Open-loop aileron, elevator, and throttle doublet and step data was collected to validate the predictive capability of the identified bare-airframe models.

Open-loop elevator and throttle frequency sweeps were used to collect data for longitudinal system identification because maneuvers around this axis were more stable and could be flown open-loop relatively easily. In contrast, closed-loop data was collected for lateral-directional system identification. This data can be difficult to collect open-loop because, for a small flying-wing UAS without direct yaw control, large maneuvers are typically required to adequately excite the Dutch-roll dynamics. These large maneuvers pose a risk to stability and controllability. Because of this, closed-loop testing can significantly ease flight testing and improve model accuracy.

A. Excitation Input Design

An important step of system identification flight test design is the determination of the excitation input signal. Input signals should excite the aircraft response uniformly over the desired range of frequencies. In this paper, automated frequency sweep inputs were used. Frequency sweeps were selected as they are simple to program into the autopilot in a parametric manner, and they excite the sUAS dynamics over a wide range of frequencies. Important parameters for frequency sweep design include the frequency range, signal magnitude, and signal duration. For an sUAS, these parameters may need to be adjusted for each day or even each flight based on the atmospheric conditions and the observed data quality. For example, the duration of the frequency sweep may need to be adjusted based on the prevailing wind to ensure the UAS is within the pilot's visual line of sight during the entire maneuver. The frequency sweep duration is directly related to the minimum frequency that can be identified. Practically, for an sUAS flying within VLOS, the maneuver length is recommended to be as long as the pilot can maintain VLOS for an emergent takeover if needed. Because of this, low-frequency dynamics may need to be identified using other methods, such as identification from trim data [6,38]. The frequency range should be selected to excite all rigid body modes of interest for the sUAS. The control signal magnitude should be designed to provide ample SNRs without causing responses that depart too far from the trim condition. For sUAS, larger attitude variations will likely be required than for a larger aircraft.

In addition to frequency sweeps, dissimilar inputs should be used to validate the predictive capability of the identified models to ensure that the model is not overfitted to the frequency sweep data [1]. In this paper, doublet maneuvers were used for validation tests.

Automated system identification maneuvers, including open-loop frequency sweeps, closed-loop frequency sweeps, and doublets, were implemented through modification of the ArduPlane open-source firmware. The sweeps increase exponentially in frequency over time, as described by Eqs. (11–13) [1]:

$$\delta_{\text{sweep}}[k] = A\sin(\theta_{\text{sweep}}[k]) \tag{11}$$

$$\theta_{\text{sweep}}[k] = \theta_{\text{sweep}}[k-1] + \omega_{\text{sweep}}T_s \tag{12}$$

$$\omega_{\text{sweep}} = \omega_{\text{sweep}_{\text{min}}} + 0.0187e^{4t/T_{\text{rec}}}(\omega_{\text{sweep}_{\text{max}}} - \omega_{\text{sweep}_{\text{min}}}) \tag{13}$$

where A is the signal amplitude, T_s is the sampling time, T_{rec} is the total sweep length, $\omega_{\text{sweep}_{\text{min}}}$ and $\omega_{\text{sweep}_{\text{max}}}$ are the selected minimum

Downloaded by NASA LANGLEY RESEARCH CENTER on March 17, 2025 | http://arc.aiaa.org | DOI: 10.2514/1.C038147

and maximum frequencies, t is the current time, and k is the discrete time step index.

The customized firmware allows operators to modify the parameters A, T_{rec}, $\omega_{\text{sweep}_{\min}}$, and $\omega_{\text{sweep}_{\max}}$ from ground control station (GCS) software such as Mission Planner and upload them to the autopilot in flight through radio telemetry. This lets flight test engineers design and tune system identification maneuvers in real time based on observations in the field, which can significantly improve flight test efficiency. The best choices for frequency sweep parameters such as record length and input magnitude can vary greatly depending on the visibility, wind, and turbulence at the time of the flight test. Ideally, flight tests should be performed on calm days, though this is often not possible without large delays to the flight test schedule.

B. Open-Loop Flight Test Maneuver Data Collection

Open-loop elevator and throttle frequency sweeps were performed to collect data for longitudinal frequency response estimation and model identification. During automated open-loop sweep maneuvers, manual pilot intervention may be required to keep the response near the trim condition, especially at low frequencies. To achieve this, pilot inputs were summed with excitation inputs. Experimentally, it was found that automated sweeps allow the ground-based pilot to better focus on keeping the UAS near the trim condition when compared to piloted sweeps. For best results during open-loop frequency sweep maneuvers, the following recommendations are made based on flight test experience with small flying-wing UAS.

1) Attempt to maintain trimmed straight and level flight for several seconds before and after the sweep maneuver. This allows for identification of trim parameters and easy combination of data from multiple maneuvers. This should also be done when performing doublet maneuvers.

2) Begin the sweep maneuvers at a reasonable altitude (e.g., 60 m above ground level [AGL] or higher) and ensure that the pilot can maintain a safe altitude throughout the duration of the maneuver. Certain maneuvers, such as long roll sweeps, can result in a slow loss of altitude.

3) Relaying airspeed and pitch angle information to the pilot via real-time telemetry can help ensure the UAS is operating near the same trim point for all system identification maneuvers, which will lead to a model with improved accuracy. Experimentally, it was found that an airspeed variation of about ± 2 m/s and trim pitch attitude variation of about ± 5 deg led to good modeling results. These variations are generally much smaller during closed-loop maneuvers than open-loop maneuvers.

4) Frequency sweep parameters are suggested to be adjusted based on monitored telemetry data. For example, the control input magnitude could be adjusted to ensure ample SNR and a response that stays near the trim condition. In this work, the best results were achieved when sizing open-loop inputs to roll and pitch excursions of ± 20 and ± 10 deg on relatively calm days. Other parameters, such as maneuver length and minimum frequency, may also need to be adjusted to ensure successful completion of the maneuver and capture of aircraft modal frequencies.

5) If the primary or off-axis response begins to deviate well past the recommendations in the previous two points, the pilot can intervene with brief inputs. For a small UAS, this can be a significant task that is easier to perform during automated sweeps when the pilot does not also have to perform the sweep maneuvers themselves. The use of brief, pulsed, or stepped inputs increases the likelihood that the pilot will not significantly distort the frequency content of the inputs, which could degrade modeling results.

6) The use of highly coupled inputs can hinder the system identification process. For a flying-wing UAS, minimizing the number of off-axis inputs required to keep the aircraft at trim will increase the data quality due to the increased coupling between roll and pitch. Experimentally, it was found that engaging the off-axis controller (i.e., proportional-integral-derivative [PID] pitch or roll hold controllers) during frequency sweeps resulted in comparatively lower quality data.

7) Flying with a headwind during all maneuvers can improve consistency in trim conditions and allow for an increased record time given airspace constraints by means of a reduced ground speed.

C. Closed-Loop Flight Test Maneuver Data Collection

System identification maneuvers can also be conducted during closed-loop flight. Historically, this has only been performed when required, as closed-loop testing has some disadvantages. Primarily, active feedback control will suppress the excitation signal and cause correlation between the input signal and noise in the feedback measurements. However, closed-loop testing also improves the stability and repeatability of flight maneuvers and allows for the identification of the bare-airframe, closed-loop, and broken-loop system dynamics from the same data set. These benefits are especially of interest for sUAS due to their unique challenges during system identification flight tests. Increased stability during flight tests allows for the execution of larger-amplitude flight maneuvers without losing control, resulting in sufficient SNRs for accurate identification results. Additionally, closed-loop flight makes it easier to repeat maneuvers at the same trim condition, which can be difficult for small UAS due to lacking or noisy real-time airspeed measurements and the large impact that small gusts and changes in wind speeds have on the sUAS airspeed and thus dynamics. Finally, the same closed-loop data set can be used to identify the bare-airframe dynamics and validate the closed-loop and broken-loop dynamics. Because of these benefits, identifying the bare-airframe dynamics from closed-loop flight data can lead to improved identification accuracy and a reduction in flight test time.

For closed-loop sUAS flight tests, simple control laws such as PID controllers can be quickly and effectively tuned in flight [16]. In this work, closed-loop flight testing for system identification is demonstrated using roll maneuvers. The proportional-derivative (PD) roll tracking controller shown in Fig. 4 was designed and implemented into the custom firmware. Integral action was not implemented as larger integrator gains will increase suppression of the low-frequency content of the control signal, and steady-state tracking is not a priority during frequency sweep maneuvers. Automated frequency sweeps were injected at the roll angle command, ϕ_c. Due to the increased stability created by the control system, piloted maneuvers could also be performed more easily than with open-loop maneuvers, which can eliminate the need to program automated maneuvers through custom software if it is infeasible for safety concerns or other reasons.

The flight test procedure for closed-loop maneuvers is largely the same as that previously described for open-loop maneuvers. However, the increased stability created by the feedback control system will greatly improve the ease and consistency of performing flight maneuvers. Typically, the pilot will not have to intervene to maintain stability or off-axis responses, and the UAS will remain closer to the reference flight condition during the maneuver than with open-loop maneuvers. As a result, the primary considerations are to ensure that the airspeed and pitch angle are near the desired trim condition before initiating the maneuver and to size the amplitude of the reference signal to ensure ample SNR. For a flying-wing sUAS without direct yaw control, roll maneuvers should be sized based on the yaw rate and side-acceleration response, which will have lower SNR than the roll rate response.

D. Trim Data and Phugoid Oscillation Data Collection

It is often difficult to accurately identify the phugoid mode from frequency domain data, as the low-frequency dynamics are typically poorly excited by excitation inputs such as frequency sweeps. This

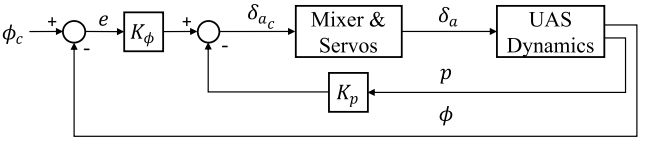

Fig. 4 Roll tracking control system diagram.

Downloaded by NASA LANGLEY RESEARCH CENTER on March 17, 2025 | http://arc.aiaa.org | DOI: 10.2514/1.C038147

Downloaded by NASA LANGLEY RESEARCH CENTER on March 17, 2025 | http://arc.aiaa.org | DOI: 10.2514/1.C038147

can lead to poor accuracy of the identified phugoid mode and longitudinal speed stability (LSS) derivatives, X_u, Z_u, and M_u. To account for this, different flight test techniques can be used to collect data to assist with modeling of the low-frequency phugoid mode dynamics. In this work, two methods for identifying the phugoid mode from flight data are demonstrated and compared.

During open-loop flight, the phugoid mode can be observed in the time domain from oscillations in speed and pitch angle measurements following an excitation input such as an elevator pulse or throttle step [3]. Analysis of prior Zephyr3-R flight test data showed that phugoid mode oscillations could be observed during straight and level flight following a turn, without an additional excitation input. This is most likely due to the dynamics being excited by throttle and elevator inputs made by the pilot to achieve a steady-state condition following the turn. For example, the pilot typically quickly decreased the throttle level when entering straight and level flight following a turn. As such, during system identification flight tests, the pilot trimmed the vehicle following a turn and flew straight and level for 15–25 s with no or minimal inputs to ensure a full oscillation cycle could be observed. Speed and pitch angle measurements during these oscillation periods were then used for phugoid mode identification.

Alternatively, the LSS derivatives can be identified from trim data recorded at several different airspeeds to identify the change in vehicle states and controls, such as pitch angle and elevator deflection, with changes in airspeed. These derivatives have a significant impact on the phugoid mode of the identified longitudinal model. By computing the LSS derivatives this way and estimating the remaining longitudinal state matrix parameters from frequency sweep data, it can be ensured that the identified longitudinal model accurately captures both the phugoid and short-period dynamics. This data can be collected open- or closed-loop. For sUAS like the Zephyr3-R, closed-loop operation can improve LSS data quality by rejecting disturbances and increasing the maximum achievable duration of straight and level flight. As such, trim data for LSS derivative estimation was collected in the "Fly-by-Wire-A" flight mode of ArduPlane, which utilizes PID controllers to track and hold a desired roll and pitch angle. The pilot controlled the throttle manually and commanded the pitch angle to ensure a near-zero rate of climb. Trim data was collected for at least 10 s. This process was repeated to collect trim data at several different airspeeds.

E. Servo Model Bench Test

In addition to flight tests, bench tests can be performed to identify the servomotor dynamics. Ideally, control surface deflection would be measured directly in flight and used as the control input signal for modeling. For sUAS, however, it is often difficult or impractical to do so due to size and weight constraints. Furthermore, sUAS are often equipped with low-cost servos that may have a bandwidth lower than the maximum frequency of flight test maneuvers required to ensure dynamic modes are accurately identified, so the servo dynamics cannot be ignored. In this case, the servo dynamics can be determined from bench tests and accounted for in the system identification process. Otherwise, the identified model parameters will be affected by the servo dynamics. Consequently, the bare-airframe dynamic modes may be biased, and the identified stability derivatives may not correspond with bare-airframe values identified from other methods such as wind tunnel testing.

In this work, servo dynamics were identified from measurements of the elevon deflection angle during bench tests. Frequency sweep signals were injected at the aileron and elevator commands, and the elevon deflection was measured by fixing an IMU to the surface. Frequency responses were estimated from the measured deflection and command signals for aileron and elevator commands. A first-order transfer function model was fit to the frequency response:

$$\frac{\delta_{a,e}}{\delta_{a,e_c}} = K_{\delta_{a,e}} \frac{1}{\tau_{\text{srv}} s + 1} \tag{14}$$

Table 2 Servo model parameters

Command	$K_{\delta_{a,e}}$, rad	τ_{srv}, s	Bandwidth, rad/s
Aileron	0.235	0.032	31.2
Elevator	0.236	0.032	31.2

where $K_{\delta_{a,e}}$ is the steady-state gain and τ_{srv} is the servo time constant, δ_{a,e_c} is the commanded aileron or elevator deflection in normalized units between ± 1, and $\delta_{a,e}$ is the measured deflection in radians. Parameter identification results are shown in Table 2. The identified models are nearly identical, as is expected based on the elevon mixing equations. Because the commands are normalized, $K_{\delta_{a,e}}$ is also equal to the maximum elevon deflection due to an aileron or elevator command, which is 13.5 deg. Time delay was not included in the servo model because measurements were synchronized manually. More information on the servo modeling bench tests can be found in [6].

V. Model Identification Approaches

This section outlines the approaches used for model identification from the collected flight data set. Frequency response and parameter identification techniques for open- and closed-loop flight data are discussed. Two phugoid mode identification approaches are also presented. These methods were used to supplement the frequency response-based identification techniques and provide verification of the identified phugoid mode dynamics.

A. Frequency Response Estimation

The theories of frequency response measurement and estimation have been widely studied and applied in many different fields [1,2,25]. Best practices depend on whether the system is operating in open- or closed-loop and on the type of excitation signal used. Spectral estimation techniques are effective when using nonperiodic excitation signals such as frequency sweeps and are discussed in the proceeding section.

1. *Open-Loop Flight Data*

Under open-loop conditions, frequency responses can be measured directly from the input and output signals using spectral estimation methods. The frequency response from input u to output y is computed as

$$\hat{G}_{uy}(j\omega) = \frac{\hat{S}_{uy}(j\omega)}{\hat{S}_{uu}(j\omega)} \tag{15}$$

where $\hat{S}_{uy}(j\omega)$ and $\hat{S}_{uu}(j\omega)$ are estimates of the input–output cross-spectrum and input autospectrum. This estimate, sometimes called the H_1 solution, is unbiased so long as there is no input noise and is the best linear approximation of the underlying nonlinear system for arbitrary inputs in a least-squares sense [25,39]. In the presence of input noise, the estimate becomes biased, and the bias errors are dependent on the input SNR (an input SNR of 3 corresponds to a bias error of around 10% [1]). The power spectra in Eq. (15) can be estimated effectively from Fourier-transformed data using the composite windowing method discussed in [1].

2. *Closed-Loop Flight Data*

Under closed-loop conditions, Eq. (15) becomes biased due to correlation between the input and output noise, which is caused by feedback. The bias can be avoided using a joint input–output estimate of the frequency response [23–25,40].

$$\hat{G}_{uy}(j\omega) = \frac{\hat{G}_{r_c y}(j\omega)}{\hat{G}_{r_c u}(j\omega)} = \frac{\hat{S}_{r_c y}(j\omega)}{S_{r_c u}(j\omega)} \tag{16}$$

where $\hat{G}_{r_c y}(j\omega)$ is the frequency response from a reference signal to the output and $\hat{G}_{r_c u}(j\omega)$ is the frequency response from the reference

Downloaded by NASA LANGLEY RESEARCH CENTER on March 17, 2025 | http://arc.aiaa.org | DOI: 10.2514/1.C038147

to the input. These two frequency responses can be computed using Eq. (15). The JIO estimate is unbiased and is the best linear approximation for a nonlinear system operating in a closed loop if the reference signal is measured without noise [25,41]. This method can be used to estimate bare-airframe frequency responses from closed-loop flight data and to perform multi-input frequency response estimation when inputs are highly correlated [24,26,27].

The frequency response estimates in Eqs. (15) and (16) are defined for single-input data because the maneuvers flown in this work were all single-input maneuvers. However, this approach can be extended to MIMO data by replacing these equations with MIMO equivalents, such as those discussed in [1] for inputs with low correlation and [24] for highly correlated inputs caused by feedback control.

Frequency responses equivalent to the closed-loop system transfer functions in Eqs. (8–10) can be estimated from closed-loop flight data. The measured frequency responses can be compared to the transfer functions that are computed using the identified bare-airframe model and control system parameters to provide validation of the performance of the control system in flight.

Referring to the control system in Fig. 4, the roll angle-to-roll command frequency response $\phi/\phi_c(j\omega)$ can be estimated directly from measurements of the roll angle and roll command using the H_1 solution, and is equal to

$$\frac{\phi}{\phi_c}(j\omega) = \frac{G(j\omega)K_\phi}{s + G(j\omega)(K_\phi + sK_p)} \tag{17}$$

where $G(j\omega)$ is the identified roll rate-to-aileron command model $p/\delta_{a_c}(j\omega)$, which combines the bare-airframe and servo dynamics. Derivation of Eq. (17) assumes that $\phi(j\omega) \approx p(j\omega)/s$ due to small pitch angles.

To measure the stability margins, the closed loop is broken at the input to the aileron mixer. Because there are two feedback paths (roll angle and roll rate), this can be visualized more easily using an equivalent block diagram representation of the control system that has a single feedback path, shown in Fig. 5. This loop can be measured from the aileron command δ_{a_c} and the feedback signal f in Fig. 5 using Eq. (15). However, the aileron command will be corrupted with correlated noise due to feedback, which causes this direct approach to be biased. The magnitude of the bias error will be dependent on the SNR of the aileron command signal [1]. To avoid bias errors, an indirect approach can be used where the response is recovered algebraically from a measured open-loop response [1,42], or the JIO approach can be used to estimate the frequency response. The JIO approach is recommended over the indirect approach as it provides an estimate of the coherence between the input and output of interest, whereas an indirect approach will only provide coherence information about a different input–output pair and recover magnitude and phase information algebraically. Using the JIO approach, the loop broken at the aileron actuator is estimated by

$$\frac{f}{\delta_{a_c}}(j\omega) = \left[\frac{f}{\phi_c}(j\omega)\right]\left[\frac{\delta_{a_c}}{\phi_c}(j\omega)\right]^{-1} = (K_\phi/s + K_p)G(j\omega) \tag{18}$$

Lastly, the roll sensitivity function is measured from the loop broken at the roll angle measurement feedback. As discussed with Eq. (10), this loop can be estimated directly from the roll error, $e = \phi_c - \phi$, and roll command using the H_1 solution, or it can be equivalently computed from the closed-loop transfer function $\phi/\phi_c(j\omega)$ from Eq. (17).

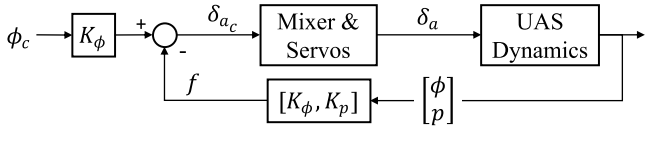

Fig. 5 Equivalent block diagram for the roll tracking controller.

$$\frac{e}{\phi_c}(j\omega) = [1 + G(j\omega)(K_\phi/s + K_p)]^{-1} = 1 - \frac{\phi}{\phi_c}(j\omega) \tag{19}$$

As with the bare-airframe frequency response estimates, the closed-loop and broken-loop equations can be solved using matrix representations. The broken loop at the actuator will be an $N_u \times N_u$ frequency response matrix, where N_u is the number of control inputs. The closed-loop response and sensitivity function will be $N_y \times N_{r_c}$ matrices, where N_y and N_{r_c} are the numbers of outputs and reference signals. The equivalent theoretical responses in Eqs. (8–10) will be transfer function matrices of the same sizes.

3. Coherence

The coherence function is often used to assess the quality of a frequency response, as it measures the linear correlation between the measured input and output as a function of frequency. Coherence is defined as [1,39]

$$\gamma^2_{uy}(j\omega) = \frac{|\hat{S}_{uy}(j\omega)|^2}{|\hat{S}_{uu}(j\omega)||\hat{S}_{yy}(j\omega)|} \tag{20}$$

In this paper, the coherence of a frequency response computed using the JIO method is taken as the minimum coherence between the two frequency responses used in the calculation at each frequency. The coherence function can also be used to estimate the linearly attributable SNR [39]:

$$\mathrm{SNR}(j\omega) = \frac{\gamma^2_{uy}(j\omega)}{1 - \gamma^2_{uy}(j\omega)} \tag{21}$$

B. Parameter Identification

State space model parameter identification can be performed by fitting the model parameters to the measured frequency responses. Equations (3–7) can be written in standard state space form:

$$\dot{\boldsymbol{x}}(t) = \boldsymbol{A}\boldsymbol{x}(t) + \boldsymbol{B}\boldsymbol{u}(t - \tau) \tag{22}$$

$$\boldsymbol{y}(t) = \boldsymbol{C}\boldsymbol{x}(t) + \boldsymbol{D}\boldsymbol{u}(t - \tau) \tag{23}$$

The outputs y used for longitudinal and lateral-directional model identification are $(a_x, a_z, q, \dot{u}, \dot{w})$ and $(a_y, p, r, \dot{v})$. The model parameters of the $\boldsymbol{A}$ and $\boldsymbol{B}$ matrices can be estimated through minimization of a quadratic cost function that represents the mismatch between the model G and the frequency response estimated from flight data for each input–output pair, $\hat{G}$ [1]:

$$\bar{J} = \frac{1}{N_{FR}}\sum_{i=1}^{N_{FR}}\frac{20}{N_\omega}\sum_{k=1}^{N_\omega} W_\gamma[(|G_i(j\omega_k)| - |\widehat{G}_i(j\omega_k)|)^2 + 0.01745(\angle G_i(j\omega_k) - \angle\widehat{G}_i(j\omega_k))^2] \tag{24}$$

where N_ω is the number of frequency points, N_{FR} is the number of frequency responses, and W_γ is a weighting function based on coherence [1]. A rule of thumb states that cost function values below 50 indicate an excellent fit [1]. This cost function is best minimized using pattern search methods due to its highly nonlinear nature [1]. Other cost functions derived using a maximum likelihood framework have also been proven effective for estimating parameters from measured frequency responses [43,44].

Several metrics are commonly computed and used to assess the accuracy of estimated state space model parameters and to determine the model structure. Two common metrics are computed from estimates of the Hessian matrix of the cost function. The Cramér–Rao bound provides a theoretical limit for the possible accuracy of the estimated parameter and, after adjustment, provides an approximation of the standard deviation of the identified parameter [1,45]. Parameter insensitivities are the lower limit of the Cramér–Rao

Downloaded by NASA LANGLEY RESEARCH CENTER on March 17, 2025 | http://arc.aiaa.org | DOI: 10.2514/1.C038147

bound and measure how insensitive the cost function is to changes to a parameter [1,45]. Cramér–Rao bounds below 20% of the parameter value and insensitivities below 10% are commonly recommended for accurate models [1]. In this paper, parameters with insensitivity values above 10% were removed from the model structure if it did not significantly increase the average cost function value [1].

After parameter identification, the simulated vehicle response generated using the identified state space model can be compared with flight data in the time domain by integrating the model equations. Biases in the states, inputs, and outputs can be identified to match the flight data used for comparison, as these biases cannot be identified in the frequency domain and often change from maneuver to maneuver [1].

C. Phugoid Mode Identification

It is often difficult to achieve accurate identification of the phugoid dynamics from frequency domain data. For sUAS, this can be caused by poor excitation of low frequencies as a result of practical limits on the maximum record time associated with VLOS flight. This can lead to poor accuracy of the identified LSS derivatives. To account for this, the phugoid mode dynamics can be identified in other ways. Two approaches are discussed below and compared later. First, the mentioned derivatives can be determined from trim data [1,38]. Second, the phugoid mode can be identified in the time domain from oscillation data using the logarithmic decrement method.

1. *LSS Derivative Identification from Trim Data*

Trim data collected at several airspeeds can be used to determine a linear relationship of the UAS states and controls with airspeed. Linear trim gradients can be fit to the data and used in conjunction with the identified state space model parameters to identify the LSS derivatives. The LSS derivatives are computed from Eq. (3) when evaluated at steady state ($\Delta\dot{x} = 0$) [1]. For example,

$$\Delta\dot{u} = X_u\Delta u + X_w\Delta w - g\cos\Theta_0\Delta\theta + X_{\delta_e}\Delta\delta_e + X_n n = 0 \quad (25)$$

$$X_u = -X_w\left(\frac{\Delta w}{\Delta u}\right) + g\cos\Theta_0\left(\frac{\Delta\theta}{\Delta u}\right) - X_{\delta_e}\left(\frac{\Delta\delta_e}{\Delta u}\right) - X_n\left(\frac{\Delta n}{\Delta u}\right) \quad (26)$$

and similarly for Z_u and M_u, where Δ indicates the change in the variable with respect to different trim conditions.

Because other state space model parameters [e.g., X_w, X_{δ_e}, and X_n in Eq. (26)] are required for computation, identifying the LSS derivatives is an iterative process. The LSS derivatives should be fixed, then the remaining state space parameters estimated from frequency responses, then the LSS derivatives should be recomputed, and this should be repeated until the results converge. This process is preferred to identifying the speed derivatives directly from frequency responses, as the low-frequency content needed to accurately estimated these derivatives is typically not available in the response data [1,38]. For example, Z_u may be identified with a positive sign, which corresponds to a negative steady-state lift coefficient for low-speed UAS flight.

2. *Time-Domain Phugoid Mode Identification*

The phugoid dynamics can also be measured directly from oscillations observed in the UAS airspeed or ground speed and pitch angle collected during flight. This motion can be excited with inputs such as a throttle step or elevator pulse [3]. The damping ratio ζ, damped natural frequency ω_d, and undamped natural frequency ω_n can then be computed from the oscillation data using the logarithmic decrement method for underdamped systems [46]:

$$\zeta = \frac{\ell_n(z_2/z_1)}{\sqrt{\ell_n(z_2/z_1)^2 + 4\pi^2}} \quad (27)$$

$$\omega_d = \frac{2\pi}{T_{12}} \quad (28)$$

$$\omega_n = \frac{\omega_d}{\sqrt{1-\zeta^2}} \quad (29)$$

where z_2 and z_1 are the amplitudes of subsequent peaks and T_{12} is the period of oscillation measured as the time between two peaks. The phugoid mode dynamics identified using this approach can be compared to the dynamics of the state space model identified from the frequency responses and LSS gradients.

VI. Flight Test Results

This section details system identification results from flight test data. First, system identification results are presented for the bare-airframe longitudinal UAS dynamics, which were identified from open-loop frequency sweep data and LSS data. The phugoid dynamics were also identified from time-domain oscillation data and compared with the frequency response- and LSS-based results. Then, lateral-directional modeling results are presented to demonstrate the closed-loop system identification approach. Frequency responses were identified for the lateral-directional bare-airframe, closed-loop, and broken-loop dynamics from the same data set. In this work, frequency response and parameter estimation were performed using the approaches discussed in Sec. V. with the commercial software package CIFER® [1]. Finally, this section concludes with a discussion on the tradeoffs between open-loop and closed-loop flight testing for sUAS system identification.

A. Identification of Longitudinal Bare-Airframe Dynamics

The primary flight data used for identification of the bare-airframe longitudinal dynamics were open-loop elevator and throttle frequency sweeps. UAS time-history data during an automated elevator sweep is shown in Fig. 6. The commanded elevator and elevator deflection are compared. The high-frequency portion of the frequency sweep causes noticeable attenuation of the elevator command, demonstrating the importance of accurately identifying and accounting for the servo dynamics. An example throttle maneuver is shown in Fig. 7. The motor speed response to the throttle command is relatively slow, illustrating the importance of directly measuring the motor speed. The flight test procedure for the elevator and throttle sweeps is discussed in further detail in [4,6].

In addition to frequency sweep data, trim data was collected during closed-loop flight at several different airspeeds to support identification of the LSS derivatives. One set of LSS trim data is shown in Fig. 8, and the linear trim gradients, which were fit from multiple trim datasets using ordinary least squares, are shown in Fig. 9.

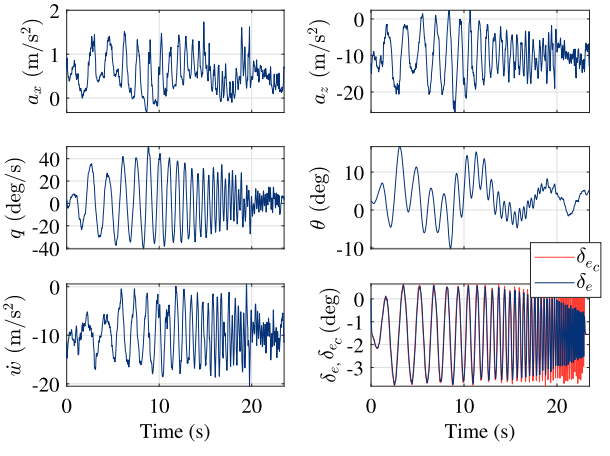

Fig. 6 Time history of elevator sweep maneuver.

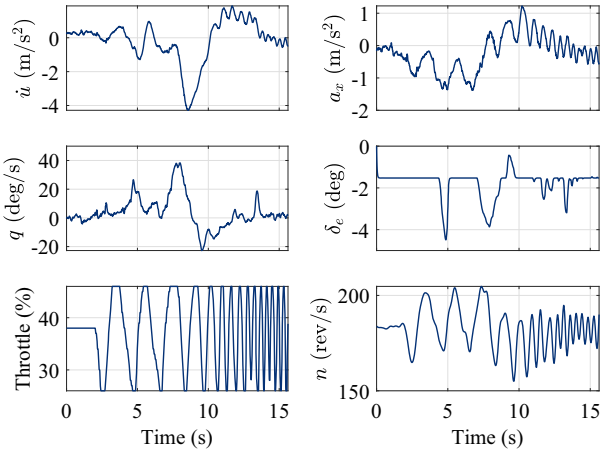

Fig. 7 Time history of throttle sweep maneuver.

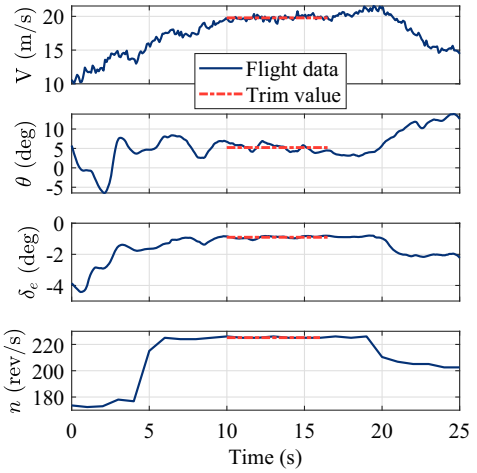

Fig. 8 Example longitudinal speed stability data.

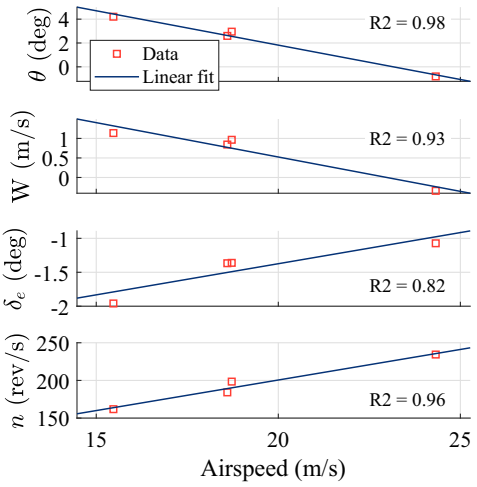

Fig. 9 Trim gradients determined from LSS data.

Frequency responses were estimated to model the UAS response to elevator and motor speed inputs. Five longitudinal responses to the elevator and two responses (a_x and $\dot{u}$) to motor speed were used for model identification. State space model parameters were estimated to minimize the error between the modeled and measured frequency responses at frequencies with high coherence. The measured and modeled frequency responses are plotted in Fig. 10. Each model fits well with the measured response, as indicated by the low individual cost function values. The response to motor speed was identified over a relatively narrow band, which could be improved if longer flight data records are collected.

The identified dynamic modes and state space model parameters are listed in Tables 3 and 4. All identified parameters are shown to have high accuracy as indicated by the Cramér–Rao bounds and insensitivities, which are all below or near recommended values. The parameters Z_q, X_{δ_e}, and M_n were removed from the model structure because of large insensitivity values, indicating that these parameters have a negligible effect on the UAS dynamics. Because of the low sampling rate of the motor speed measurements, the associated time delay may be inflated by up to the sampling period of 0.1 s.

The predictive capability of the identified state space model was checked against flight data in the time domain. A sample pitch doublet and a throttle step maneuver are shown in Figs. 11 and 12. The model accurately predicts the response to both control inputs. The Theil inequality coefficient (TIC), which represents the normalized root mean square error between the model and data, is 0.10 and 0.18 for the two maneuvers. Values below 0.25 generally indicate high accuracy [3].

The phugoid mode dynamics were also identified directly in the time domain to verify the results from the state space model identification. Flight data was collected with the sticks fixed to observe oscillations in the ground speed and pitch angle. Ground speed was used rather than airspeed as the measurements were less noisy, which made it easier to identify peaks in the oscillations. Seven peak-to-peak oscillations were measured and averaged to determine the phugoid dynamics. One example of a phugoid oscillation time history is shown in Fig. 13. The data was processed with a zero-phase low-pass filter to reveal smooth peaks in the oscillation. A linear trend line was fit to the data, and the time between two peaks, T_{12}, and the difference between the peaks and the trend line, z, were measured to compute the phugoid mode damping coefficient and natural frequencies using Eqs. (27–29). Subtracting out the trend line removes bias and drift in the data. The response appears linear and second order, as demonstrated by the exponential decay of oscillations and relatively constant time between peaks.

The time-domain identified phugoid mode is compared to the state space model, which was estimated from frequency responses and LSS data, in Table 5. The 2σ value is shown in parentheses for the time domain results. The natural frequencies show excellent agreement with each other, indicated by very low percentage errors. The time domain-identified damping coefficient has higher variance and percent error, but still shows good agreement with the frequency domain result. All frequency domain-identified parameters are within the 2σ bound of the time domain results.

B. Identification of Lateral-Directional Bare-Airframe, Closed-Loop, and Broken-Loop Dynamics

Closed-loop flight testing was conducted to identify the lateral-directional system dynamics. The roll controller shown in Fig. 4 was implemented, and reference frequency sweeps were injected at the roll command, ϕ_c, with an amplitude of ± 15 deg. Time history data from one frequency sweep maneuver is shown in Fig. 14. The angular rate and control surface deflections are large in magnitude, peaking at ± 100 deg/s and ± 9 deg; however, the roll angle stays within the desired ± 15 deg range. The large magnitude inputs result in high SNR throughout the duration of the maneuver. Furthermore, the airspeed variance is low, remaining near 20.5 m/s for the entire maneuver, which can be difficult to achieve during open-loop sweep maneuvers for this UAS. In Table 6, the standard deviation σ of the airspeed, pitch angle, and roll angle and the SNR of the input–output responses are compared to data from similar open-loop frequency sweep maneuvers from prior work [4]. SNR and trim condition variance provide a nonparametric method of comparing data quality between two data sets collected at different flight conditions, which complicates comparisons between model parameters. The SNR was estimated from the coherence function between 1.5 and 25 rad/s. Overall, closed-loop testing led to data with lower deviation from the flight condition and higher SNRs when compared to the open-loop

Downloaded by NASA LANGLEY RESEARCH CENTER on March 17, 2025 | http://arc.aiaa.org | DOI: 10.2514/1.C038147

Downloaded by NASA LANGLEY RESEARCH CENTER on March 17, 2025 | http://arc.aiaa.org | DOI: 10.2514/1.C038147

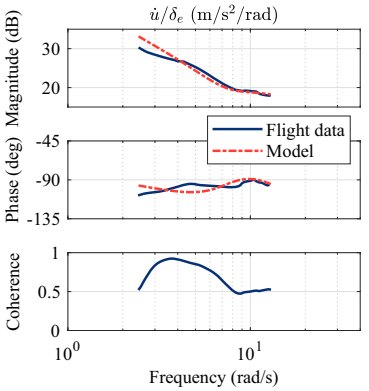

a) X-axis body velocity derivative-to-elevator, $\dot{u}/\delta_e$, model fit (J = 29.9)

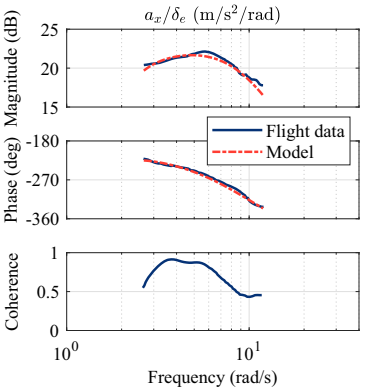

b) Longitudinal acceleration-to-elevator, a_x/δ_e, model fit (J = 3.6)

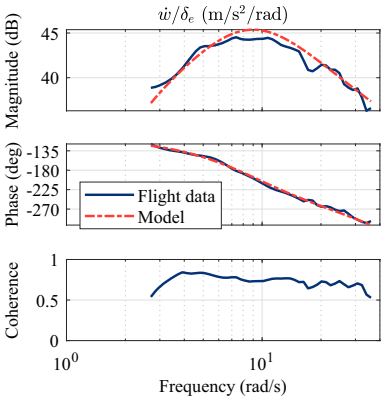

c) Z-axis body velocity derivative-to-elevator, $\dot{w}/\delta_e$, model fit (J = 10.5)

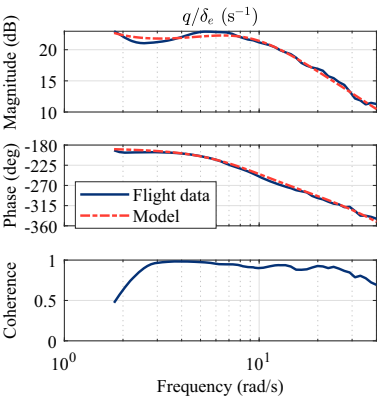

d) Pitch rate-to-elevator, q/δ_e, model fit (J = 7.7)

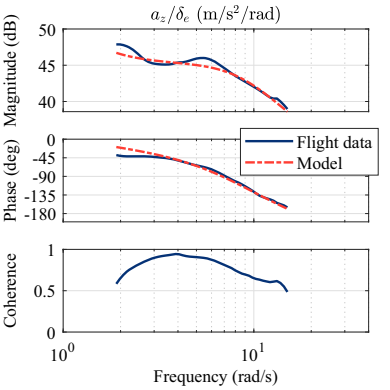

e) Vertical acceleration-to-elevator, a_z/δ_e, model fit (J = 20.4)

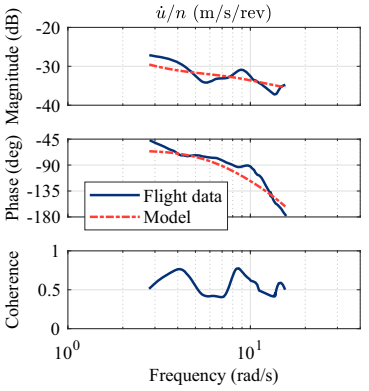

f) X-axis body velocity derivative-to-motor speed, $\dot{u}/n$, model fit (J = 55.9)

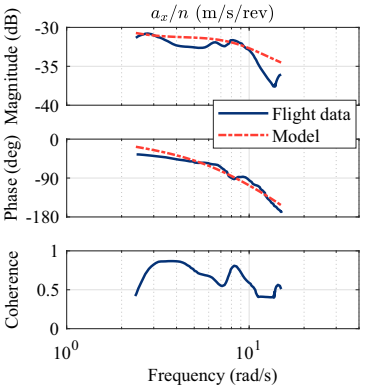

g) Longitudinal acceleration-to-motor speed, a_x/n, model fit (J = 35.5)

Fig. 10 Longitudinal state space model fit (J = 23.4).

Table 3 Identified longitudinal dynamic modes

Dynamic mode	Poles	Damping coefficient	Natural frequency, rad/s
Short-period	$-6.55 \pm 5.91j$	0.74	8.82
Phugoid	$-0.102 \pm 0.803j$	0.13	0.809

results. Five roll command sweeps of similar quality were collected during one flight, whereas the data used in [4] was collected over several flights on different days, indicating the ease of collecting data under closed-loop conditions. This same data set was used to identify the bare-airframe and closed-loop system dynamics.

1. Bare-Airframe Model Identification

Bare-airframe frequency responses for roll rate, yaw rate, lateral acceleration, and lateral velocity derivative were estimated from the flight data using the JIO method. State space model parameters were estimated to minimize the error between the modeled and measured frequency responses at frequencies with high coherence. The computed frequency responses are shown in Fig. 15 and compared with the identified state space model. Each of the four frequency responses matches well with the model. The responses exhibit high coherence over a wide frequency band, indicating the high quality of the data and highly linear response despite the large control deflections and angular rates. The identified lateral-directional model parameters are listed in Table 7. The parameters L_v, Y_r, and Y_{δ_a} were removed from the model structure due to high insensitivity.

Table 4 Longitudinal state space model parameters

Parameter	Unit	Value	Cramér–Rao bound, %	Insensitivity, %
X_u[a]	s^{-1}	−0.1090	— —	— —
X_w	s^{-1}	0.5500	7.4	1.3
X_q	m/s	−0.3182	22.7	5.2
Z_u[a]	s^{-1}	−3.045	— —	— —
Z_w	s^{-1}	−6.805	5.3	1.5
M_u[a]	$(m \cdot s)^{-1}$	−0.1464	— —	— —
M_w	$(m \cdot s)^{-1}$	−2.041	11.0	2.7
M_q	s^{-1}	−6.395	12.7	1.7
X_n	$m/(rev \cdot s)$	0.01321	17.5	3.2
Z_{δ_e}	m/s^2	−30.26	22.0	7.3
Z_n	$m/(rev \cdot s)$	0.2270	16.8	3.1
M_{δ_e}	rad/s^2	−132.9	5.3	1.0
τ_{δ_e}	s	0.0398	6.2	2.5
τ_n	s	0.1507	6.7	1.7

[a]Speed derivatives determined from the LSS method and fixed during identification of other parameters.

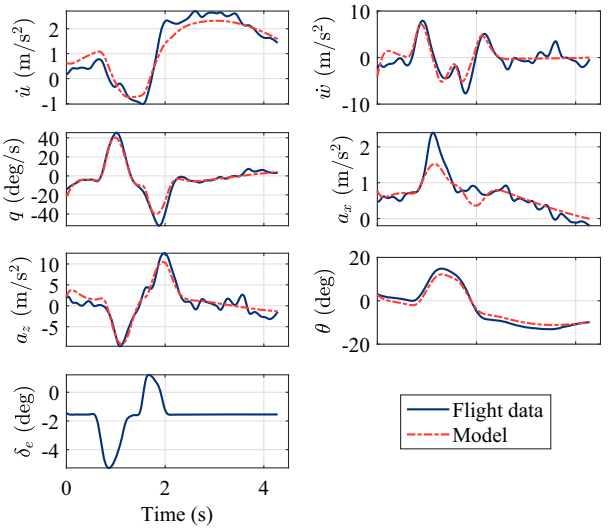

Fig. 11 Elevator doublet time domain validation results (TIC = 0.10).

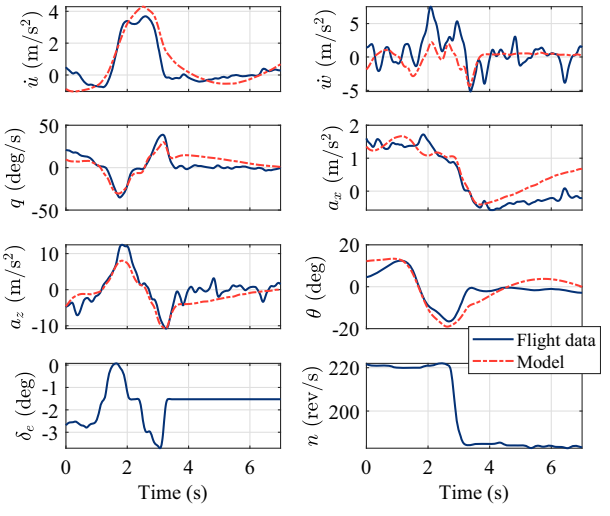

Fig. 12 Throttle step time domain validation results (TIC = 0.18).

The majority of the remaining parameters were identified with low variance, as indicated by the Cramer–Rao bounds. Two terms, L_r and N_p, were identified with Cramer–Rao bounds and insensitivities near or above typical guidelines. This may be a result of the rudderless flying-wing configuration, which makes it more difficult to excite yawing motion. If a rudder surface was available, the L_v, L_r, and N_p derivatives would likely be identifiable and important for accurate modeling. Despite the increased variance, inclusion of these parameters was found to result in a more accurate model with better predictive capability. The identified dynamic modes are listed in Table 8.

The identified state space model was compared against flight data in the time domain to verify the predictive capability of the model. Flight data and the model-predicted response of an aileron doublet are shown in Fig. 16. The model accurately predicts the response to the control input and nonzero initial conditions, which is characterized by a TIC value of 0.12. This maneuver also demonstrates the susceptibility of the UAS to wind and turbulence due to its small size and lack of yaw control, which is one challenge of collecting system identification data for this sUAS. At the beginning of the data record, the roll angle and rate are zero; however, the Dutch-roll mode is excited, as indicated by the oscillations and nonzero initial conditions in yaw rate and side acceleration.

2. *Closed-Loop and Broken-Loop System Identification*

The closed-loop and broken-loop frequency responses discussed previously were identified from the same flight data as the bare-airframe model and frequency responses. The measured frequency responses were compared to the identified model transfer functions. The cost function in Eq. (24) was computed between 1 and 30 rad/s to quantify the match between the model and data. The measured roll command-to-roll angle frequency response is compared against the model in Fig. 17. The closed-loop system model matches the flight data closely, as indicated by the low cost function value. The loop broken at the aileron actuator was estimated using the JIO approach in Eq. (18), which ensures that the frequency response is unbiased, and is shown in Fig. 18. When little noise is present, as indicated in this case by coherence values near one, the JIO and direct approaches will provide similar results. However, as noise levels increase and coherence reduces, the direct approach will exhibit more error, and so the JIO approach is preferred. In Fig. 18, the stability margins and crossover frequencies are marked with circles and diamonds. The model matches the measured response well and accurately predicts the in-flight stability margins. Finally, the roll sensitivity function is shown in Fig. 19, with the disturbance rejection bandwidth and peak marked. Again, the model accurately predicts the response and the in-flight disturbance rejection metrics. A full comparison of the identified stability margins and disturbance rejection metrics is shown in Table 9. All modeled parameters are identified within 10% of the in-flight values.

These results indicate the benefits and efficiency of closed-loop flight testing for sUAS. Closed-loop flight testing simplified the data collection procedure, reduced the number of maneuvers flown to collect sufficient data for system identification, improved SNRs, and reduced the deviation of the vehicle from the reference flight condition during frequency sweep maneuvers. From the same flight data set, the bare-airframe dynamics were accurately identified in addition to three important frequency responses that describe the closed-loop and broken-loop system dynamics. The closed-loop and broken-loop frequency responses estimated from flight data matched closely with the modeled responses. Overall, closed-loop flight testing led to highly accurate models and improved the simplicity, repeatability, and efficiency of system identification flight testing.

C. Discussion and Recommendations

There are several factors that influence the decision to collect open-loop or closed-loop flight data for sUAS system identification. The primary consideration is the level of difficulty in collecting high-quality system identification data using each approach. The

Downloaded by NASA LANGLEY RESEARCH CENTER on March 17, 2025 | http://arc.aiaa.org | DOI: 10.2514/1.C038147

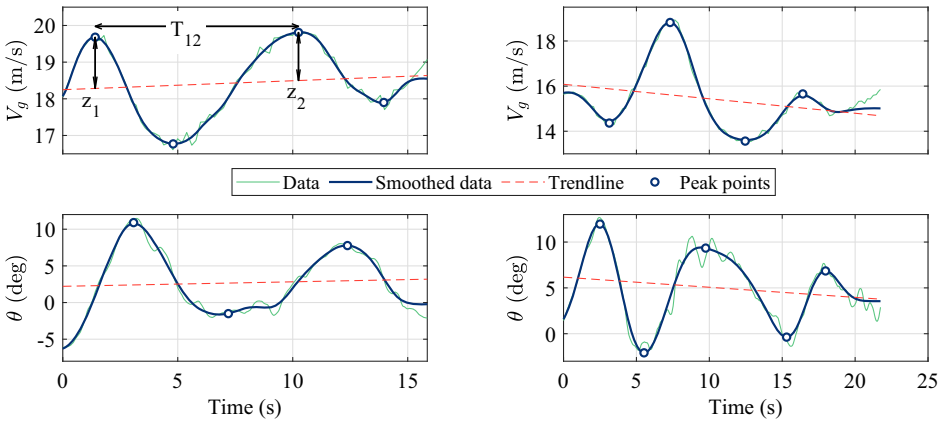

Fig. 13 Phugoid oscillation data.

Table 5 Comparison of phugoid mode identification results

Parameter	State space model	Time-domain identification	Percent error, %
Damped natural frequency, rad/s	0.755	0.719 (±0.075)	4.8
Undamped natural frequency, rad/s	0.809	0.759 (±0.074)	6.2
Damping coefficient	0.13	0.10 (±0.08)	23

Table 6 Comparison of open- and closed-loop flight maneuver data

Parameter	Open-loop data	Closed-loop data	Percent change, %
$\sigma(V_a)$, m/s	2.3	0.64	−72
$\sigma(\theta)$, deg	4.3	1.1	−74
$\sigma(\phi)$, deg	16.5	8.0	−52
SNR $(\dot{v}/\delta_a)$	4.3	6.9	60
SNR (p/δ_a)	12.2	15.7	29
SNR (r/δ_a)	3.4	10.3	203
SNR (a_y/δ_a)	2.9	8.5	193

level of difficulty will largely depend on the aircraft configuration and size and the experience of the flight crew.

For certain sUAS, such as those with conventional configurations or larger weights or wingspans, open-loop system identification maneuvers can be performed readily and easily. In this case, the open-loop approach is recommended for bare-airframe system identification, as the disadvantages of closed-loop operation (e.g., suppression of excitation and correlated noise) would outweigh any potential advantages. For example, for the sUAS in this paper, elevator and throttle frequency sweep maneuvers were easy to perform open-loop. For this reason, and to demonstrate the system identification procedure using open-loop data, open-loop maneuvers were flown for short-period mode identification, while the phugoid mode was identified separately from LSS data.

The closed-loop approach is recommended for sUAS that face challenges maintaining stability and controllability when performing system identification maneuvers or maintaining a flight condition during the duration of a maneuver. For example, for the rudderless flying-wing sUAS in this paper, large amplitude roll maneuvers were required to sufficiently excite the Dutch-roll dynamics. This reduced stability and caused the UAS to depart significantly from the trim condition during maneuvers. Furthermore, this aircraft is notably susceptible to wind and turbulence due to its lightweight, which also made it difficult to maintain a constant trim condition during maneuvers. As such, the data quality and system identification results were significantly improved when using closed-loop data. In general, more aggressive control gains will lead to greater improvements in stability and flight test ease but will also cause greater suppression of the excitation and thus aircraft dynamics. As a result, a tradeoff must be made between these competing factors.

While the closed-loop approach can lead to similar or improved results compared to the open-loop method, additional work may be required of flight test engineers. For instance, the time and effort spent on controller design and input signal generation will vary depending on the specific flight test campaign. Some aircraft can be tuned easily and rapidly in flight [16], and closed-loop excitation signals could be generated by a remote control pilot. In this case, closed-loop flight testing for system identification is more accessible than in other situations. For example, if the number of inputs to the airframe is larger than the number of available pilot inputs, additional considerations will be required to ensure that the bare-airframe inputs can be excited in a decorrelated manner. This can be achieved by using computer-generated signals injected at the bare-airframe input or by repeating piloted maneuvers with different

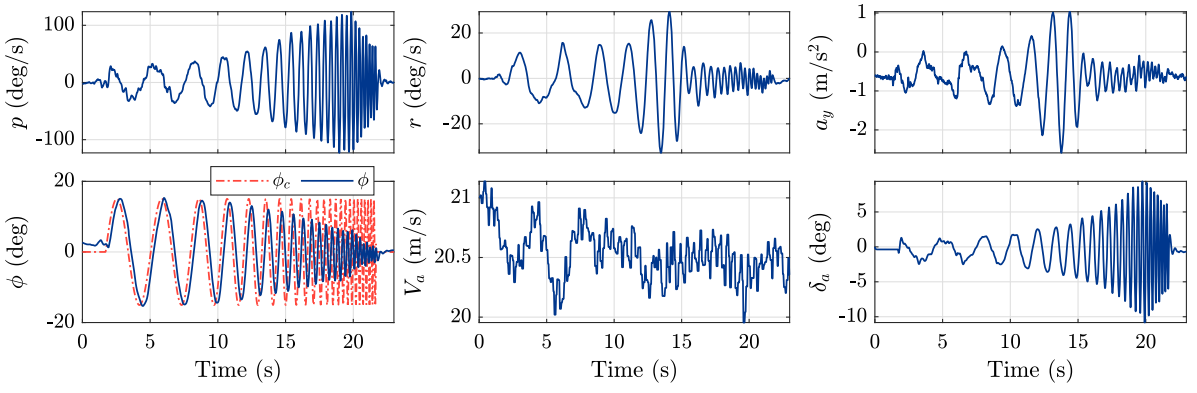

Fig. 14 Roll command sweep time history data.

Downloaded by NASA LANGLEY RESEARCH CENTER on March 17, 2025 | http://arc.aiaa.org | DOI: 10.2514/1.C038147

Downloaded by NASA LANGLEY RESEARCH CENTER on March 17, 2025 | http://arc.aiaa.org | DOI: 10.2514/1.C038147

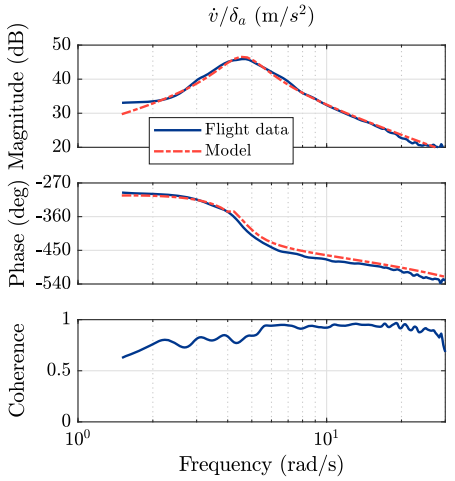

a) Y-axis body velocity derivative-to-aileron, $\dot{v}/\delta_e$, model fit (J = 13.7)

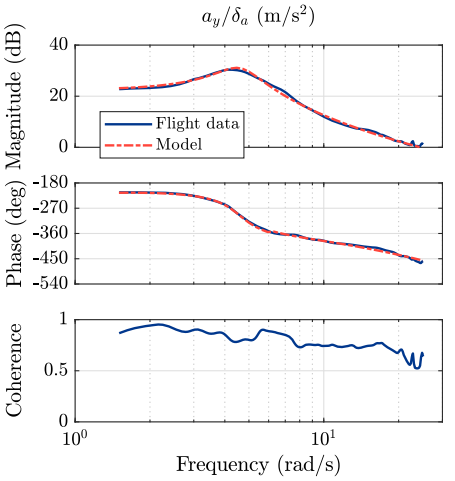

b) Side acceleration-to-aileron, a_y/δ_a, model fit (J = 15.4)

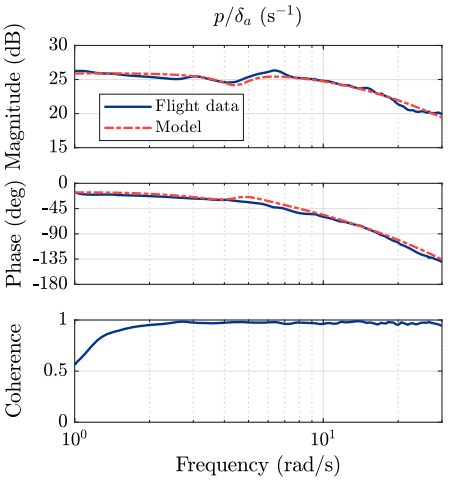

c) Roll rate-to-aileron, p/δ_a, model fit (J = 14.6)

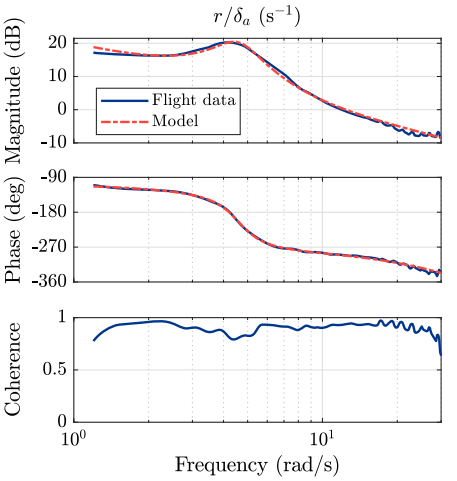

d) Yaw rate-to-aileron, r/δ_a, model fit (J = 16.0)

Fig. 15 Lateral-directional state space model fit (J = 13.4).

Table 7 Lateral-directional state space model parameters

Parameter	Unit	Value	Cramér–Rao bound, %	Insensitivity, %
Y_v	s^{-1}	−0.7626	5.9	2.5
Y_p	m/s	0.06498	17	7.5
L_p	s^{-1}	−15.21	9.7	1.9
L_r	s^{-1}	5.623	38.3	15.4
N_v	$(m \cdot s)^{-1}$	0.9736	2.5	1.1
N_p	s^{-1}	0.1219	53.6	9.8
N_r	s^{-1}	−0.8769	12.6	5
L_{δ_a}	rad/s^2	314.9	8.1	1.5
N_{δ_a}	rad/s^2	−11.6	8.0	1.6
τ_{δ_a}	s	0.04248	6.5	2.2

Table 8 Identified lateral-directional dynamic modes

Dynamic mode	Poles	Damping coefficient	Natural frequency, rad/s
Roll	−14.7	1	14.7
Dutch roll	$-0.87 \pm 4.5\ j$	0.19	4.60
Spiral	−0.17	1	0.17

control or mixer gains [27,28]. In contrast, closed-loop testing will typically reduce pilot workload when flying system identification maneuvers, which may be important for pilots who have less experience with system identification flight testing. Safety concerns and procedures may also affect the time spent on control system design, and there are extra considerations during data analysis when working with closed-loop data. All these factors should be considered when designing a flight test plan.

Finally, the closed-loop approach can be used to identify bare-airframe models and validate the implementation of the closed-loop system from the same data set. This advantage can reduce total flight testing time, especially as it becomes more common for sUAS to be equipped with open-source autopilots that have control laws that can be tuned in-flight. If flight testing time is limited, collecting closed-loop system identification data may be preferable to open-loop testing, even if there are no other difficulties collecting the data open-loop.

VII. Conclusions

This paper presented methods for sUAS system identification using open-loop or closed-loop flight data. Flight test procedures were developed for both approaches to address the challenges of sUAS system identification, including flight test design for various system identification flight maneuvers. The open-loop method entails estimating bare-airframe frequency responses from open-loop system

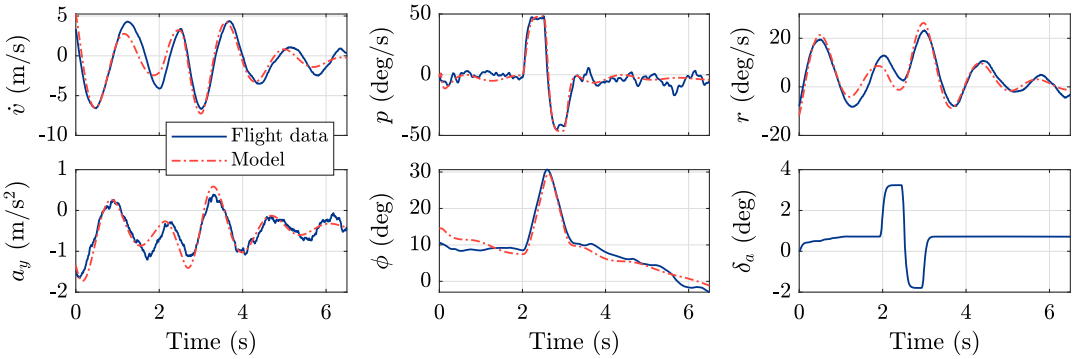

Fig. 16 Aileron doublet time domain validation results (TIC = 0.12).

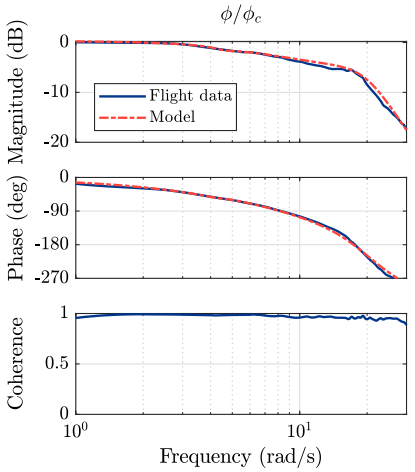

Fig. 17 Roll angle-to-roll command frequency response model comparison ($J = 9.2$).

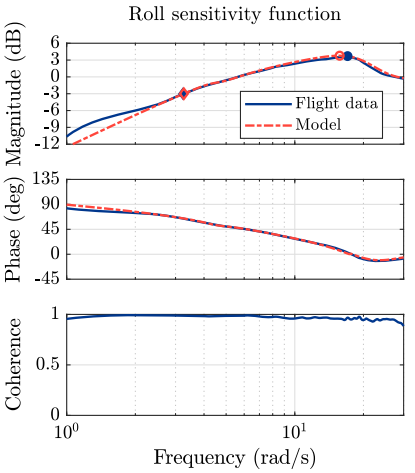

Fig. 19 Roll sensitivity function model comparison ($J = 20.0$).

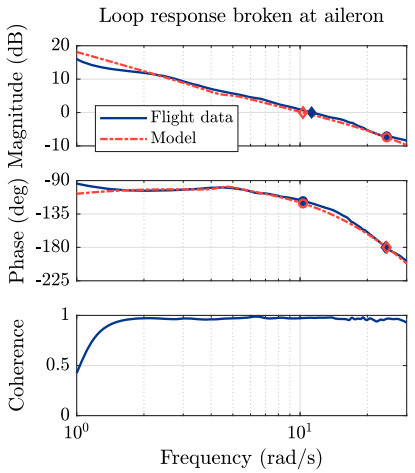

Fig. 18 Loop response broken at aileron actuator model comparison ($J = 24.9$).

identification maneuver data, which was collected with the KHawk Zephyr3-R UAS. A linear state space model representing the longitudinal UAS dynamics was identified from measured frequency response data and trim data. The longitudinal speed stability derivatives, which significantly impact the phugoid mode of the model, were identified from trim data, while the remaining parameters were estimated from frequency responses. The phugoid mode was also identified from measured oscillations in the UAS velocity and pitch angle during steady-state flight. This approach showed excellent agreement with the identified linear model, validating the accuracy of the identified phugoid dynamics with time-history data, which has not been demonstrated in the literature for sUAS at this scale.

Table 9 Stability margin parameter identification results

Parameter	Flight data	Model	Percent error, %
Gain margin, dB	7.1	7.4	4.7
Phase margin, deg	62.4	59.1	5.2
Gain crossover frequency, rad/s	11.3	10.3	8.5
Phase crossover frequency, rad/s	24.1	24.4	1.4
Disturbance rejection bandwidth, rad/s	3.2	3.3	0.8
Disturbance rejection peak, dB	3.7	3.8	1.9
DRP frequency, rad/s	17.0	15.7	7.7

Additionally, the closed-loop method was developed to improve the stability, repeatability, and efficiency of sUAS system identification flight testing. Using this method, the bare-airframe, closed-loop, and broken-loop dynamics can be accurately identified from the same set of closed-loop flight data. These benefits can lead to a reduction in the required number of flight maneuvers and thus the cost, duration, and efforts of system identification flight testing. Closed-loop roll command frequency sweep maneuvers were flown to collect data that was used to estimate frequency responses and identify a linear state space model representing the lateral-directional UAS dynamics. The model was then compared with closed- and broken-loop frequency responses estimated from the same flight data set. The results showed excellent agreement, with all computed parameters, such as stability margins, matching within 10%, indicating the effectiveness of the described methods.

The results of this work can facilitate the field of sUAS system identification and other research areas that would benefit from experimental model identification procedures, such as computational aerodynamic parameter estimation, control system and state estimator design, and wind and turbulence estimation. Future research directions

Downloaded by NASA LANGLEY RESEARCH CENTER on March 17, 2025 | http://arc.aiaa.org | DOI: 10.2514/1.C038147

include comparison of estimated stability and control derivatives with computational methods, identification of dynamic motor models, and identification of bare-airframe models at different trim conditions in support of a full flight-envelope model, which would have a wider range of applicability than a state space model linearized at a single trim point. The developed procedures are shown to be highly repeatable, which will improve the efficiency of this type of flight testing. Future demonstrations of this method on vertical takeoff and landing aircraft could also prove useful due to their increasingly widespread use and inherent instability, which necessitates closed-loop testing.

Acknowledgment

The authors would like to thank the Associate Editor, the two anonymous reviewers, and Dr. Tom Berger from the U.S. Army DEVCOM Aviation & Missile Center for providing comments to improve the quality of the paper. This paper was partially sponsored by the Army Research Laboratory under Cooperative Agreement Number W911NF-22-2-0207. This work was also supported in part by the NASA-KS-EPSCoR Grant R53187-23-01419 and the USDA-NIFA Grant 2019-67021-28992. The views and conclusions contained in this document are those of the authors and should not be interpreted as representing the official policies, either expressed or implied, of the Army Research Laboratory or the U.S. Government. The U.S. Government is authorized to reproduce and distribute reprints for Government purposes notwithstanding any copyright notation herein.

References

[1] Tischler, M. B., and Remple, R. K., *Aircraft and Rotorcraft System Identification: Engineering Methods with Flight-Test Examples*, 2nd ed., AIAA, Reston, VA, 2012.

[2] Morelli, E. A., and Klein, V., *Aircraft System Identification: Theory and Practice*, 2nd ed., Sunflyte Enterprises, Williamsburg, VA, 2016.

[3] Jategaonkar, R. V., *Flight Vehicle System Identification: A Time Domain Methodology*, 2nd ed., AIAA, Reston, VA, 2012.

[4] Matt, J. J., Hagerott, S. G., Svoboda, B. C., Chao, H., and Flanagan, H. P., "Frequency Domain System Identification of a Small Flying-Wing UAS," *AIAA SciTech Forum*, AIAA Paper 2022-2407, 2022. https://doi.org/10.2514/6.2022-2407

[5] Flanagan, H. P., Hagerott, S. G., and Chao, H., "Model Based Roll Controller Tuning and Analysis for Small UAS in Turbulent Environments," *2018 International Conference on Unmanned Aircraft Systems (ICUAS)*, Inst. of Electrical and Electronics Engineers, New York, 2018, pp. 1398–1407. https://doi.org/10.1109/ICUAS.2018.8453442

[6] Matt, J. J., Chao, H., Shawon, M. H., and Hagerott, S. G., "Longitudinal System Identification for a Small Flying-Wing UAS," *AIAA SciTech Forum*, AIAA Paper 2023-0628, 2023. https://doi.org/10.2514/6.2023-0628

[7] Simmons, B. M., McClelland, H. G., and Woolsey, C. A., "Nonlinear Model Identification Methodology for Small, Fixed-Wing, Unmanned Aircraft," *Journal of Aircraft*, Vol. 56, No. 3, 2019, pp. 1056–1067. https://doi.org/10.2514/1.C035160

[8] Dorobantu, A., Murch, A., Mettler, B., and Balas, G., "System Identification for Small, Low-Cost, Fixed-Wing Unmanned Aircraft," *Journal of Aircraft*, Vol. 50, No. 4, 2013, pp. 1117–1130. https://doi.org/10.2514/1.C032065

[9] Woodrow, P., Tischler, M., Mendoza, G., Hagerott, S. G., and Hunter, J., "Low Cost Flight-Test Platform to Demonstrate Flight Dynamics Concepts Using Frequency-Domain System Identification Methods," *AIAA Atmospheric Flight Mechanics (AFM) Conference*, AIAA Paper 2013-4739, 2013. https://doi.org/10.2514/6.2013-4739

[10] Babcock, J. T., Osteroos, R. K., and Tischler, M. B., "Open and Closed Loop System Identification of the Stryker 200 UAV," *AIAA SciTech Forum*, AIAA Paper 2022-2405, 2022. https://doi.org/10.2514/6.2022-2405

[11] Venkataraman, R., and Seiler, P., "System Identification for a Small, Rudderless, Fixed-Wing Unmanned Aircraft," *Journal of Aircraft*, Vol. 56, No. 3, 2019, pp. 1126–1134. https://doi.org/10.2514/1.C035141

[12] Sanders, F. C., Tischler, M., Berger, T., Berrios, M. G., and Gong, A., "System Identification and Multi-Objective Longitudinal Control Law Design for a Small Fixed-Wing UAV," *AIAA Atmospheric Flight Mechanics Conference*, AIAA Paper 2018-0296, 2018. https://doi.org/10.2514/6.2018-0296

[13] Simmons, B. M., Gresham, J. L., and Woolsey, C. A., "Flight-Test System Identification Techniques and Applications for Small, Low-Cost, Fixed-Wing Aircraft," *Journal of Aircraft*, Vol. 60, No. 5, 2023, pp. 1503–1521. https://doi.org/10.2514/1.C037260

[14] Matt, J. J., and Chao, H., "Efficient Frequency Response Identification for Small Fixed-Wing UAS Using Closed-Loop Flight Data," *AIAA SciTech 2023 Forum*, AIAA Paper 2023-0629, 2023. https://doi.org/10.2514/6.2023-0629

[15] Grauer, J. A., "Frequency Response Estimation for Multiple Aircraft Control Loops Using Orthogonal Phase-Optimized Multisine Inputs," *Processes*, Vol. 10, No. 4, 2022, p. 619. https://doi.org/10.3390/pr10040619

[16] Matt, J. J., Flanagan, H., and Chao, H., "Evaluation and Analysis of ArduPilot Automatic Tuning Algorithm for the Roll Tracking Controller of a Small UAS," *AIAA SciTech Forum*, AIAA Paper 2021-0016, 2021. https://doi.org/10.2514/6.2021-0016

[17] Cunningham, M., and Hubbard, J. E., "Open Loop System Identification of a Small Multirotor Vehicle with an Active Feedback Control System," *AIAA Atmospheric Flight Mechanics Conference*, AIAA Paper 2018-3475, 2018. https://doi.org/10.2514/6.2018-3475

[18] Sun, S., de Visser, C. C., and Chu, Q., "Quadrotor Gray-Box Model Identification from High-Speed Flight Data," *Journal of Aircraft*, Vol. 56, No. 2, 2019, pp. 645–661. https://doi.org/10.2514/1.C035135

[19] Alabsi, M. I., and Fields, T. D., "Real-Time Closed-Loop System Identification of a Quadcopter," *Journal of Aircraft*, Vol. 56, No. 1, 2019, pp. 324–335. https://doi.org/10.2514/1.C034219

[20] Niermeyer, P., Raffler, T., and Holzapfel, F., "Open-Loop Quadrotor Flight Dynamics Identification in Frequency Domain via Closed-Loop Flight Testing," *AIAA Guidance, Navigation, and Control Conference*, AIAA Paper 2015-1539, 2015. https://doi.org/10.2514/6.2015-1539

[21] Wei, W., Cohen, K., and Tischler, M. B., "System Identification and Controller Optimization of a Quadrotor UAV," *AHS 71st Annual Forum*, American Helicopter Soc. Paper F-0071-2015-10298, 2015. https://doi.org/10.4050/F-0071-2015-10298

[22] Gong, A., Sanders, F. C., Hess, R. A., and Tischler, M. B., "System Identification and Full Flight-Envelope Model Stitching of a Package-Delivery Octocopter," *AIAA SciTech Forum*, AIAA Paper 2019-1076, 2019. https://doi.org/10.2514/6.2019-1076

[23] Akaike, H., "Some Problems in the Application of the Cross-Spectral Method," *Advanced Seminar on the Spectral Analysis of Time Series*, Wiley, Hoboken, NJ, 1967, pp. 81–107.

[24] Berger, T., Tischler, M. B., Knapp, M. E., and Lopez, M. J. S., "Identification of Multi-Input Systems in the Presence of Highly Correlated Inputs," *Journal of Guidance, Control, and Dynamics*, Vol. 41, No. 10, 2018, pp. 2247–2257. https://doi.org/10.2514/1.G003530

[25] Pintelon, R., and Schoukens, J., *System Identification: A Frequency Domain Approach*, 2nd ed., Wiley, Hoboken, NJ, 2012.

[26] Knapp, M. E., Berger, T., Tischler, M., and Cotting, M. C., "Development of a Full Envelope Flight Identified F-16 Simulation Model," *AIAA Atmospheric Flight Mechanics Conference*, AIAA Paper 2018-0525, 2018. https://doi.org/10.2514/6.2018-0525

[27] Berrigan, C., Lopez, M. J. S., Ruckel, P., and Prasad, J. V. R., "Bell V-280 System Identification and Model Validation with Flight Test Data Using the Joint Input-Output Method" *VFS 76th Annual Forum*, Vertical Flight Soc. Paper F-0076-2020-16393, 2020. https://doi.org/10.4050/F-0076-2020-16393

[28] Berger, T., Lopez, M. J. S., and Tischler, M. B., "Guidelines for System Identification of Multirotor Vehicles with Highly Correlated Inputs," *VFS 76th Annual Forum*, Vertical Flight Soc. Paper F-0076-2020-16294, 2020. https://doi.org/10.4050/F-0076-2020-16294

[29] Lopez, M., Tischler, M., Juhasz, O., Gong, A., Sanders, F., and Walan, A., "Development of a Reconfigurable Multicopter Flight Dynamics Model from Flight Data Using System Identification," *8th Biennial Autonomous VTOL Technical Meeting*, Vertical Flight Soc. Paper sm_8VTOL_2019_26_Lopez, 2019.

[30] Grauer, J. A., and Boucher, M. J., "Real-Time Estimation of Bare-Airframe Frequency Responses from Closed-Loop Data and Multisine Inputs," *Journal of Guidance, Control, and Dynamics*, Vol. 43, No. 2, 2020, pp. 288–298. https://doi.org/10.2514/1.G004574

Downloaded by NASA LANGLEY RESEARCH CENTER on March 17, 2025 | http://arc.aiaa.org | DOI: 10.2514/1.C038147

[31] Tischler, M. B., Berger, T., Ivler, C. M., Mansur, M. H., Cheung, K. K., and Soong, J. Y., *Practical Methods for Aircraft and Rotorcraft Flight Control Design: An Optimization-Based Approach*, AIAA, Reston, VA, 2017, pp. 113–114, 148–149, 200.

[32] McRuer, D., Ashkenas, I., and Graham, D., *Aircraft Dynamics and Automatic Control*, Princeton Univ. Press, 1973.

[33] Roskam, J., *Airplane Flight Dynamics & Automatic Flight Controls: Part I*, DARcorporation, Lawrence, KS, 1995.

[34] Rahmani, S., Wang, Z., Matt, J. J., Lin, Z., Chao, H., Zheng, Z., Keshmiri, S., and Ewing, M., "Comparison of Low- and High-Fidelity CFD Based Estimates of Forces, Moments, and Aerodynamic Coefficients with UAS Flight Test Data," *AIAA AVIATION Forum*, AIAA Paper 2022-4065, 2022. https://doi.org/10.2514/6.2022-4065

[35] Anon., "Flying Qualities of Piloted Aircraft," U.S. Dept. of Defense Rept. MIL-HDBK-1797B, Washington, D.C., April 2012.

[36] Berger, T., Ivler, C., Berrios, M., Tischler, M., and Miller, D., "Disturbance Rejection Handling Qualities Criteria for Rotorcraft," *AHS 72nd Annual Forum*, American Helicopter Soc. Paper F-0072-2016-11452, 2016. https://doi.org/10.4050/F-0072-2016-11452

[37] Blanken, C. L., Hoh, R. H., Mitchell, D. G., and Key, D. L., "Test Guide for ADS-33E-PRF," US Army RDECOM, Special Report AMR-AF-08-07, Moffett Field, CA, July 2008.

[38] Berger, T., Tischler, M. B., Hagerott, S. G., Christopher Cotting, M., and Gray, W. R., "Identification of a Full-Envelope Learjet-25 Simulation Model Using a Stitching Architecture," *Journal of Guidance, Control, and Dynamics*, Vol. 43, No. 11, 2020, pp. 2091–2111. https://doi.org/10.2514/1.G005094

[39] Bendat, J. S., and Piersol, A. G., *Engineering Applications of Correlations and Spectral Analysis*, Wiley, New York, 1980, pp. 173–190.

[40] Ljung, L., *System Identification: Theory for the User*, 2nd ed., Prentice Hall, Upper Saddle River, NJ, 1999, pp. 434–440.

[41] Pintelon, R., and Schoukens, J., "FRF Measurement of Nonlinear Systems Operating in Closed Loop," *IEEE Transactions on Instrumentation and Measurement*, Vol. 62, No. 5, 2013, pp. 1334–1345. https://doi.org/10.1109/TIM.2012.2220033

[42] McCoy, A. H., "Flight Testing and Real-Time System Identification Analysis of a UH-60A Black Hawk Helicopter with an Instrumented External Sling Load," M.S. Thesis, Dept. of Aeronautical Engineering, Naval Post Graduate School, 1997.

[43] Grauer, J. A., "Dynamic Modeling Using Output-Error Parameter Estimation Based on Frequency Responses Estimated with Multisine Inputs," NASA TM 2018-220108, Nov. 2018.

[44] Grauer, J. A., and Boucher, M. J., "Aircraft System Identification from Multisine Inputs and Frequency Responses," *Journal of Guidance, Control, and Dynamics*, Vol. 43, No. 12, 2020, pp. 2391–2398. https://doi.org/10.2514/1.G005131

[45] Maine, R. E., and Illif, K. W., "The Theory and Practice of Estimating the Accuracy of Dynamic Flight-Determined Coefficients," NASA RP-1077, July 1981.

[46] Iman, D. J., *Engineering Vibration*, 2nd ed., Pearson Education, Upper Saddle, NJ, 2008, pp. 59–61.

T. Strganac
Associate Editor

Downloaded by NASA LANGLEY RESEARCH CENTER on March 17, 2025 | http://arc.aiaa.org | DOI: 10.2514/1.C038147